Received: 3 February 2021 | Revised: 11 March 2021 | Accepted: 21 March 2021

DOI: 10.1002/cey2.115

REVIEW

CARBON ENERGY WILEY

Modulating charge carriers in carbon dots toward efficient solar-to-energy conversion

Namhee Kim[1] | Jiyoung Lee[1] | Minsu Gu[2] | Byeong-Su Kim[1]

[1]Department of Chemistry, Yonsei University, Seoul, Republic of Korea

[2]Department of Chemical Engineering (BK21 FOUR), Dong-A University, Busan, Republic of Korea

Correspondence

Minsu Gu, Department of Chemical Engineering (BK21 FOUR), Dong-A University, Busan 49315, Republic of Korea.
Email: sbgms@dau.ac.kr

Byeong-Su Kim, Department of Chemistry, Yonsei University, Seoul 03722, Republic of Korea.
Email: bskim19@yonsei.ac.kr

Funding information

National Research Foundation of Korea, Grant/Award Numbers: NRF-2017M3A7B4052802, NRF-2018R1A5A1025208

Abstract

Growing attention to the development of sustainable solar-to-energy conversion applications has resulted in the synthesis of promising and environment-friendly nanomaterials as energy harvesters. Among various carbon nanomaterials, carbon dots (CDs) have received significant attention due to their excellent light absorption capability, broad absorption region, and superior photostability with enormous potential for solar energy applications. Therefore, utilizing and modulating the charge carriers generated from CDs is critical for achieving a high energy conversion efficiency of CDs. Herein, we focus on the distinct characteristics of CDs as energy converters from charge excitation to charge separation and transfer for various solar-to-energy applications, including photovoltaic cells, photocatalysts, and photoelectrocatalysts. We anticipate that this review will offer insight into the synthesis and design of novel nanocomposites with a fundamental analysis of the photochemical properties and future development of energy conversion devices.

KEYWORDS

carbon dots, charge carrier, energy conversion, photocatalyst, photoelectrocatalyst

1 | INTRODUCTION

Carbon dots (CDs) have received widespread attention in the scientific community as one of the latest additions to carbon-based nanomaterials. CDs, which are typically defined as quasi-spherical carbon nanoparticles of <10 nm, exhibit unique physical, chemical, and optical properties, including high light absorption, tunable photoluminescence, and excellent electron donor/acceptor characteristics.[1–6] Owing to these advantages, CDs can be applied in bioimaging,[7,8] biosensing,[9–11] drug delivery,[12–15] phototherapy,[16–18] and light-harvesting applications in energy transducers.[19–21]

Moreover, the facile and mild synthetic nature of CDs using various combinations of carbon precursors and other molecular agents can provide easy access to the formation of sp^2-hybridized carbonaceous core of CDs, with an amorphous shell rich in surface functional groups containing oxygen and nitrogen. These surface functional moieties can be potentially functionalized with other organic molecules on the CD surface, allowing the control of photoluminescence (PL)

Namhee Kim and Jiyoung Lee contributed equally to this study.

and photocatalytic activities of CDs. With the increasing demand for renewable solar-to-energy applications in future, it is important to fully utilize the photoexcited charge carriers generated from CDs and reveal the specific role of CDs as energy converters for the development of efficient conversion devices. Although many studies[22–24] have tried to achieve a high energy conversion efficiency of CDs by hybridizing them with various counterpart nanomaterials to afford CD nanocomposites, the photo-responsibilities of CDs extensively depend on the nanoscale size, type, amount of heteroatom doping, surface functionality, and assembled nanocomposites. In addition, the slower kinetics and mobilities of charge carriers in CDs than those in other inorganic semiconductors (i.e., quantum dots [QDs]) have limited their practical applications. Furthermore, it is still relatively unexplored to provide a general method on how to separate and transfer electrons and holes effectively due to the intrinsic complexity of CDs. In the context of using CDs in high-performance energy conversion applications, it is, therefore, necessary to understand a stepwise mechanism of the charge carriers of CDs upon light irradiation: (1) charge excitation: a large number of electron–hole pairs should be produced from the surface of CDs; (2) charge separation: these electron–hole pairs should be separated efficiently into free electrons and holes, respectively, against Coulombic attraction; (3) charge transfer: separated electrons and holes should be effectively transferred and participate in the respective target reactions (i.e., electrons for cathodic and holes for anodic reactions) required for specific energy applications.

Although there are many excellent reviews[25–29] on CD-based nanocomposites, there are only a few methodically organized reviews focusing on the perspective of charge carriers in CDs from charge generation to transfer, and eventually to energy applications. Therefore, herein we introduce strategies to efficiently utilize the photoexcited charge carriers from CDs by classifying them into three steps: (i) charge excitation, (ii) charge separation, and (iii) charge transfer for various solar-to-energy applications, including photovoltaic cells, photocatalysts, and photoelectrocatalysts (Figure 1). We anticipate that our insight will be beneficial for modulating the charge carriers in CDs toward the development of advanced sensors and electronic and energy devices.

2 | CHARGE EXCITATION

In this section, we describe the light absorption properties of CDs in the course of charge excitation process toward the energy conversion application. Moreover, the

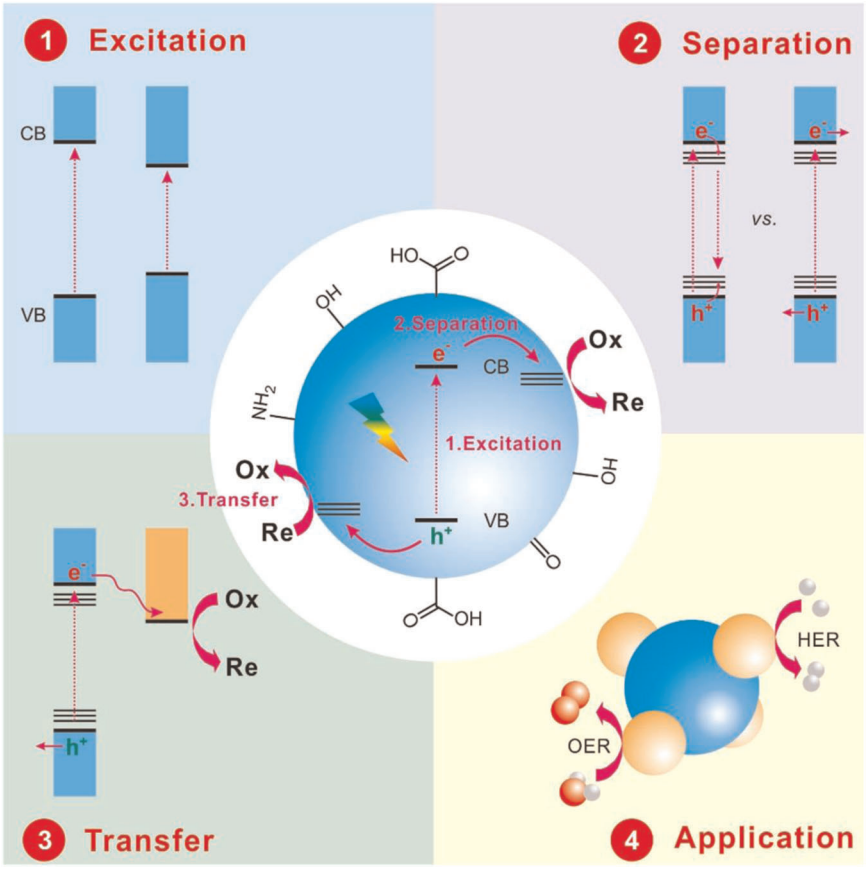

FIGURE 1 Schematic illustration of a stepwise process that efficiently modulates the photoexcited charge carriers of CDs from (1) excitation to (2) separation and (3) transfer toward (4) solar-to-energy conversion applications. CD, carbon dot; HER, hydrogen evolution reaction; OER, oxygen evolution reaction

surface modification and the band gap tuning of CDs are discussed in terms of their applicability in a wide range of photophysical and photochemical processes.

2.1 | Light absorption

CDs have been highlighted as efficient light-absorbing materials owing to their excellent properties, such as high absorption activity, broad absorption region, and superior photostability. The chemical structure and composition of CDs significantly affect their absorption abilities. The absorption spectrum of CDs represents an absorption band in the 230–320 nm UV region, attributed to the π–π^* transition of the π-conjugated electrons in the sp^2-hybridized region, and an absorption band around 350 nm, assigned to the n–π^* transitions of O- and/or N-containing structures at the edge.[30–32] Besides these two bands, a long absorption tail extending into the visible region is typically related to functional groups with lower energy states. Surprisingly, CDs exhibit a large molar extinction coefficient from 1×10^4 to $20 \times 10^4\ M^{-1}{\cdot}cm^{-1}$ in the UV region, which is higher than that of common fluorophores and is comparable to that of semiconducting QDs.[33,34] For comparison, Ru-based dyes, known as standard sensitizers, possess a molar extinction coefficient of $1.4 \times 10^4\ M^{-1}{\cdot}cm^{-1}$, with an order of magnitude lower than that of CDs.[35,36] The graphitization and core nitrogen doping of CDs are related to their high absorption coefficient. Martindale et al.[37] reported that graphitized and nitrogen-doped CDs exhibit enhanced light absorption as compared with amorphous CDs, improving the photochemical performance owing to their light-harvesting ability as photosensitizers (Figure 2A,B).

Conventional light-absorbing materials such as $BiPO_4$ and ZnO are excited only under UV radiation, which accounts for 4% of the total solar energy. In addition, the organic dyes show discrete absorption bands with a narrow absorption range.[41] However, CDs exhibit unique optical absorption properties, such as the broad absorption bands in full-range UV and visible light, and the two-photon absorption to expand the absorption coverage of solar spectrum. Whereas the downconversion PL of CDs is generally observed, upconversion PL is also observed in some cases due to abundant surface functional groups, extending the light absorption from UV to visible light range. Cao et al.[7] first reported that the CDs prepared by laser ablation display upconversion PL properties, exhibiting strong luminescence for two-photon excitation in the near-infrared region. In addition, the two-photon excitation mechanism was revealed to elucidate the upconversion PL.

Moreover, CDs have excellent photostability as compared with conventional organic dyes, such as fluorescein and rhodamine B, due to their chemical composition with extensive π-conjugated regions in the core and various functional groups on the surface.[42] Liu et al.[43] reported that the fluorescence intensity of N-CDs preserved up to 96% under UV radiation with an intensity of $20\ mW{\cdot}cm^{-2}$. The photostability of N-CDs was attributed to the steric effect of the nitrogen-doping agent with abundant dendritic hydroxymethyl groups. The diffusion of oxygen into the fluorescence centers could be effectively slowed down, thus protecting the degradation induced by photooxidation.

2.2 | Semiconducting properties

Photon absorption produces an exciton, that is, the excitation of electron from the valence band (VB)/highest occupied molecular orbital (HOMO) to the conduction band (CB)/lowest unoccupied molecular orbital (LUMO). Many researchers have suggested that the molecular orbital theory can be applied to the electronic structures of CDs with semiconducting properties.[44–48] In most cases, CDs can easily produce n–π^* and π–π^* transitions. If the functional groups are bonded to the aromatic sp^2-hybridized region, electron transitions can occur from the n states of the electron lone pairs to the π^* states of the aromatic region. The band gap of CDs induced by conjugated π-domains and the surface/edge state can be adjusted by modulating the size and surface chemistry. In this section, we describe the tunable band gap properties of the CDs.

The band gap of the CDs is theoretically size-dependent, and the red shift of the emission wavelength appears with an increase in size. Sk et al.[34] systematically investigated the influence of size on the band gap of CDs using density functional theory and time-dependent density functional theory. They revealed that the emission wavelength of the CDs shifted from UV to near infrared with increasing size. In addition, they observed that CDs with various edge configurations exhibited different quantum confinement effects. Whereas the armchair edge counterparts widened the band gap due to the localized states scattered in the center, the zigzag edge configurations exhibited a relatively narrow band gap owing to the localized states scattered in the edge.

The band gap and PL properties of the CDs can be significantly affected by surface modification and passivation, which employ various agents, such as small molecules and polymers. Tetsuka et al.[49] designed amino-functionalized CDs produced by graphene oxide

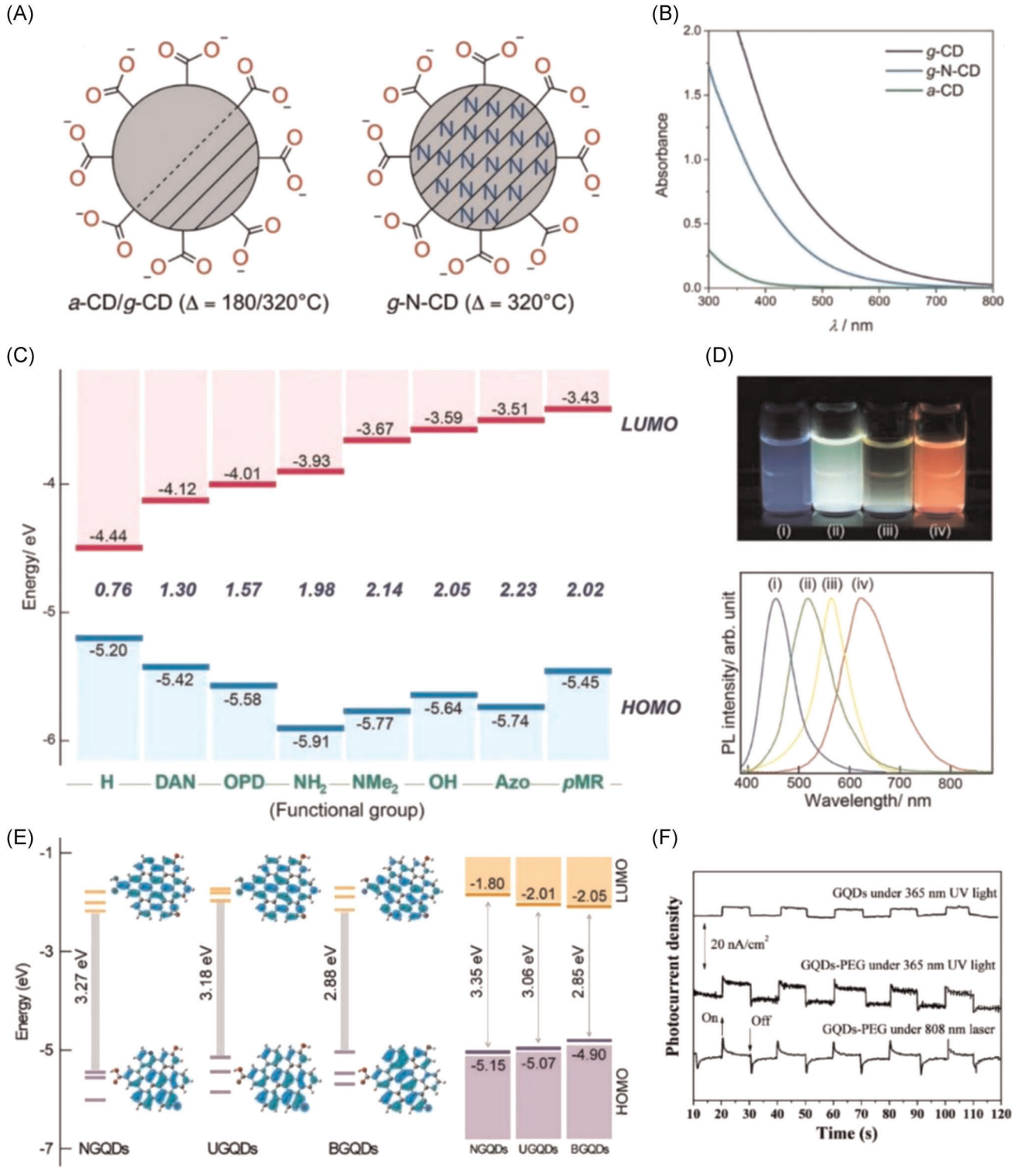

FIGURE 2 (A) Schematic representation of amorphous carbon dots (a-CD), graphitized CDs (g-CD), and graphitized and nitrogen-doped CDs (g-N-CD). Reproduced with permission: Copyright 2017, Wiley.[37] (B) UV–vis absorption spectra of g-CD, g-N-CD, and a-CD. Reproduced with permission: Copyright 2017, Wiley.[37] (C) Measured energy level diagram of nitrogen-doped CDs. Reproduced with permission: Copyright 2016, Wiley.[38] (D) Photoluminescence spectra and images of nitrogen-doped CDs under 380 and 365 nm UV-light irradiation, respectively: (i) Azo-CDs, (ii) NH_2-CDs, (iii) *o*-phenylenediamine-CDs, and (iv) diaminonaphthalene-CDs. Reproduced with permission: Copyright 2016, Wiley.[38] (E) density functional theory-simulated (left) and experimentally measured (right) energy levels of nitrogen-doped CDs (NGQDs), undoped CDs (UGQDs), and boron-doped CDs (BGQDs). Reproduced with permission: Copyright 2018, American Chemical Society.[39] (F) Photocurrent response of CD-PEG and pristine CD photoelectrodes under 365 nm UV light and 808 nm near-infrared laser. Reproduced with permission: Copyright 2012, The Royal Society of Chemistry[40]

through a mild hydrothermal treatment at 70–150°C in an ammonia solution. The covalent bonding of amine with graphene edges was achieved by nucleophilic substitution. Higher concentrations of ammonia induced a higher N/C ratio. By controlling the degree of amine functionalization, the PL properties of the CDs could be tuned from violet to yellow light. Following this study, they further investigated the influence of nitrogen-related functional groups on the energy levels and band gaps of the CDs (Figure 2C).[38] The HOMO and LUMO levels of the CDs were continuously tailored by different nitrogen moieties due to the strong orbital resonance in the graphene center. Whereas CDs modified with *o*-phenylenediamine, diaminonaphthalene, azobenzene, or *p*-methylene red displayed lower energy levels, CDs functionalized with primary or dimethylamine displayed higher energy levels. The trend in the band gaps is shown in the fluorescence spectrum (Figure 2D).

Similar to surface functionalization, heteroatom doping has been extensively used to modify the band gap and PL properties of the CDs. Yang et al.[39] studied the band gap and emissive states of heteroatom-doped CDs by comparing the spectroscopic measurements and theoretical calculations (Figure 2E). They prepared three different types of CDs with similar sizes and chemical compositions. In particular, nitrogen and boron atoms were introduced as electron-rich and electron-deficient dopants, respectively: undoped CDs, nitrogen-doped CDs (N-CDs), and boron-doped CDs (B-CDs). Compared with undoped CDs, the N-CDs and B-CDs exhibited blue- and red-shifted PL emissions, respectively. In N-CDs, the pyridinic nitrogen atom provided lone pair electrons to the occupied p orbitals, resulting in a lower HOMO level and wider band gap. In contrast, the boron atom contributes an empty orbital to the *p*-conjugated system, thus causing a decrease in the electron density of the HOMO level and narrower band gap. Mehta et al.[50] synthesized CDs by a microwave-assisted method to fabricate core–shell-type Au@CD composite. Unlike the 2.78-eV band gap of the pristine CDs, the band gap of Au@CD composite decreased to 2.68 eV owing to the charge transfer between Au and CDs, after the formation of core–shell composite.

2.3 | Generation of charge carriers

In semiconducting materials, electrons are excited to higher energy states generating electron–hole pairs. This process is called the generation of a charge carrier. CDs can generate electron–hole pairs under light irradiation with unique photoelectric properties. Shen et al.[40] synthesized poly (ethylene glycol)-passivated CDs on an indium tin oxide (ITO) substrate by a spin-coating method. The electron–hole pairs were generated and disassociated from the CDs coated on the ITO substrate under light irradiation, indicating that the CDs have an ability to produce photocurrent (Figure 2F). The measured photocurrent was extremely low; however, this study demonstrated the possibility of the application of CDs in photo-to-electric conversion.

Li et al.[51] also revealed that CDs could produce light-induced protons under visible light in an aqueous solution owing to the existence of oxygen-related functional groups. The pH dependence of CDs with or without light irradiation was photocontrollable and reversible, which is consistent with the regularity of light-induced current change, thus indicating the photo-induced proton-generating capability of CDs.

Li et al.[44] reported that CDs with size-dependent and upconversion PL properties also showed photocurrent responses in the range of 10–200 $mA \cdot cm^{-2}$. Different-sized CDs separated by column chromatography exhibited different wavelengths in the PL spectra, indicating that the current density could modulate the emission color of CDs. The lower current density induced CDs, emitting light in the longer wavelength range. The incorporation of the as-synthesized CDs with upconversion PL properties into the metal oxide also facilitated the generation of electron–hole pairs in the metal oxide. For example, in TiO_2/CDs or SiO_2/CDs nanocomposites, the CDs absorb visible light and emit a shorter wavelength light due to the upconversion PL, which, in turn, stimulates TiO_2 or SiO_2 to form electron–hole pairs.

3 | CHARGE SEPARATION

In this section, we introduce the fundamental concept of the charge recombination and charge separation process occurring in the CDs. This section also describes how to modulate the charge separation activity of CDs through surface functionalization and integration into nanocomposites.

3.1 | Charge separation efficiency

The photocatalytic activity significantly depends on the separation efficiency of photogenerated electrons and holes in various photocatalytic applications. The photogenerated electrons can return to their ground states through charge recombination, implying that the charge carrier lifetime is related to the charge separation efficiency. The charge carrier lifetime is generally defined as the average time it takes for electron–hole pairs to recombine after excitation.[52] As charge carrier lifetime is typically defined

as the statistical average time calculated by the recombination of electrons and holes through multiple pathways at different times, it is difficult to track individual charge carrier lifetimes. Thus, the lifetime (τ) has been inferred from PL,[53-55] photoconductance,[56,57] photovoltaic,[52,58] and photocatalytic[43,59–61] properties, in which generation and recombination occur. The radiative (τ_r^{-1}) and nonradiative (τ_{nr}^{-1}) recombination rates can be calculated from the photoluminescence quantum yield (PLQY), PL lifetime (τ_{PL}), and PLQY values by solving the following equations[62]:

$$\tau_{PL}^{-1} = \tau_r^{-1} + \tau_{nr}^{-1}, \quad (1)$$

$$\mathrm{PLQY} = \tau_{nr}/(\tau_r + \tau_{nr}). \quad (2)$$

Where as the radiative recombination rate shows a similar tendency to the PLQY and PL lifetimes, the nonradiative recombination rate exhibits an inverse behavior. Bhattacharyya et al.[62] revealed that there is a trade-off between PLQY and photocatalytic activity. CDs with different nitrogen contents were prepared by controlling the concentration of the nitrogen precursor. When the nitrogen content of the CDs primarily consisted of the graphitic nitrogen atoms, a high PLQY was observed. In contrast, the nitrogen-to-carbon ratios of CDs were related to nitrogen-related functional groups located at the edges of the sp^2 domains. The peripheral functionalities acted as trap states of photogenerated electrons, facilitating the charge separation that improves the photocatalytic activity.

Furthermore, the electron recombination kinetics was investigated through the transient open-circle voltage (V_{oc}) decay as a function of time after immediately turning off the light irradiation. The lifetime of the photogenerated electrons (τ_n) was calculated using the following equation:

$$\tau_n = (k_B T/e)(dV_{oc}/dt)^{-1}, \quad (3)$$

where k_B is the Boltzmann constant, T is the temperature, and e is the elementary charge.[63] Here, the lifetime (τ_n) of photogenerated electrons indirectly reflects the suppression of charge carrier recombination.

The charge carriers can be scattered or trapped by defects, increasing the probability of recombination. Therefore, the separation of photoexcited electron–hole pairs is an effective approach for inducing highly efficient photocatalysts. Many researchers have reported that the functionalization of CDs can modulate the separation efficiency of electrons and holes by increasing the charge carrier lifetime and/or tailoring the charge distribution on the CD surface. In addition, nanoscale heterojunctions with an intimate interface can significantly improve the separation of electron–hole pairs. In the CD-based nanocomposite, the photogenerated electrons from other photocatalysts can migrate into the conducting network of CDs, thereby suppressing the recombination of charge carriers at the composite interface.

3.2 | Controlling the charge separation efficiency

Tsai et al.[64] synthesized N-CDs with adjustable dopant concentrations and components. The visible absorption of N-CDs was enhanced by the introduction of C—N bonds, which created another pathway for generating PL. The time-resolved PL spectrum indicated that the carrier lifetime of CDs increased upon N doping at the optimized concentration (Figure 3A), thus leading to the highest photocurrent generation of water oxidation at 0.25 $mA{\cdot}cm^{-2}$, which is almost 10 times higher than that of the pristine CDs. Electrochemical impedance spectroscopy also demonstrated that the carrier concentration, charge dynamics, and reaction kinetics significantly increased by the N doping of CDs (Figure 3B). The combination of these factors contributed to the superior photoelectrochemical (PEC) performance and improved the photocatalytic activity of N-CDs over pristine CDs.

Hu et al.[66] also prepared Cl^- and P-doped CDs and investigated the roles of heteroatoms in photocatalytic properties. The electrochemical measurements indicated different surface potential differences between the pristine and functionalized CDs. The Cl^- and P-related functional groups could change the charge distribution of the CD surface, resulting in a higher electric potential of CDs owing to the increased number of holes trapped on the CD surface. The potential differences on the surface of the Cl^- and P-doped CDs achieved an effective separation of the photogenerated charges, facilitating enhanced photocatalytic activities.

Kong et al.[63] modified WO_3 nanoflakes with N-doped CDs (NCDs/WO_3) to develop photoanodes with high PEC activity. The conductivity was enhanced due to the N doping of CDs, representing a superior photocurrent density of 1.42 $mA{\cdot}cm^{-2}$, which is 2.25 times higher than that of pristine WO_3 nanoflakes (Figure 3C). The onset potential of NCD/WO_3 composite-based photoanode also indicated a cathodic shift of 70 mV, showing promoted charge separation and transfer owing to the NCDs acting as both electron donor and hole acceptor. The transient open-circle voltage (V_{oc}) decay was also displayed as a function of time for WO_3 nanoflakes and NCDs/WO_3, resulting in a longer lifetime (τ_n) of the NCDs/WO_3 composites than that of the pristine WO_3 nanoflakes (Figure 3D). This phenomenon indirectly reflects that the charge recombination was effectively suppressed, in

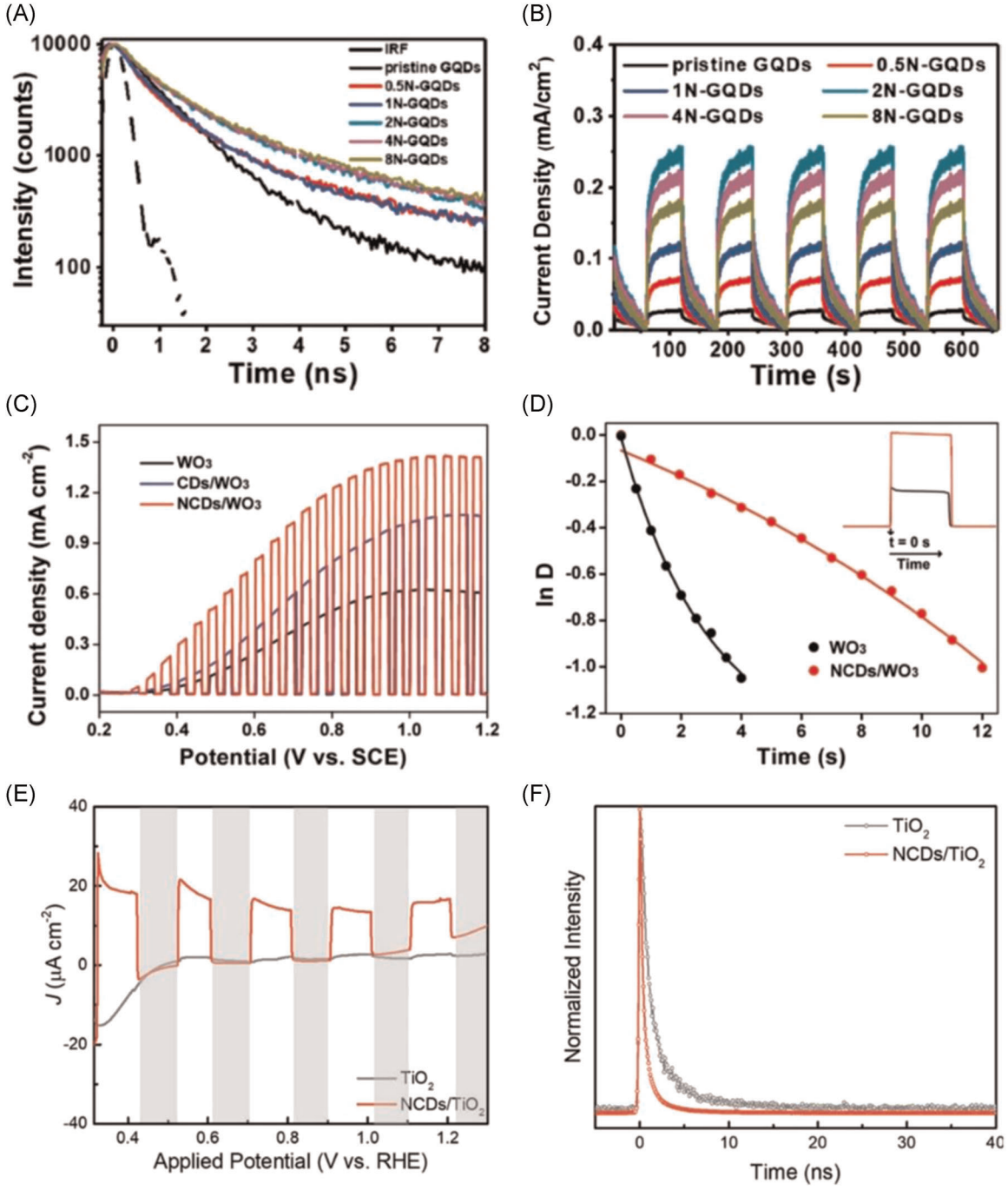

FIGURE 3 (A) Time-resolved photoluminescence spectra of pristine carbon dots (CDs) and five nitrogen-doped CDs (NCDs) recorded under 430-nm light. Reproduced with permission: Copyright 2020, American Chemical Society.[64] (B) *I–t* curves (at 1.23 V vs. reversible hydrogen electrode) of pristine CDs and five NCDs under dark and light conditions. Reproduced with permission: Copyright 2020, American Chemical Society.[64] (C) Linear sweep voltammetry (LSV) curves of pristine WO_3, CDs/WO_3, and NCDs/WO_3 photoanodes with a scan rate of 10 mV under chopped light illumination. Reproduced with permission: Copyright 2019, Wiley.[63] (D) Transient photocurrent density responses of pristine WO_3 and NCDs/WO_3 over time. Reproduced with permission: Copyright 2019, Wiley.[63] (E) The LSV curves of pristine TiO_2 and NCDs/TiO_2 under chopped visible-light illumination. Reproduced with permission: Copyright 2020, American Chemical Society.[65] (F) Time-correlated single-photon counting decay of pristine TiO_2 and NCDs/TiO_2. Reproduced with permission: Copyright 2020, American Chemical Society[65]

agreement with the transient photocurrent result. Overall, these results demonstrate that NCDs/WO_3 composites can provide an efficient strategy to improve the charge separation and transfer efficiency in PEC water oxidation.

Luo et al.[65] reported that a high photocurrent could be obtained in a PEC system by designing and manipulating CDs/TiO_2 composite. The authors systematically demonstrated the fundamental process of charge separation between NCDs and TiO_2, with an in-depth investigation of the energy transitions through the photophysical and electrochemical assays. The linear sweep voltammetry (LSV) results of the photoelectrodes showed that the saturation photocurrent of NCD/TiO_2 was observed at 0.15 mA·cm^{-2}, approximately two times higher than that of pristine TiO_2 (0.08 mA·cm^{-2}). The photogenerated charge carriers could be effectively separated owing to the formation of heterojunctions at the NCDs/TiO_2 interface. In addition, the enhanced PEC results under visible light ($\lambda > 420$ nm) agreed well with the charge separation of TiO_2 by hybridizing NCDs (Figure 3E). The carrier density (N_D) can be estimated using the following equation:

$$\frac{1}{C^2} = \frac{2}{\varepsilon\varepsilon_0 A^2 e N_D}\left(V - V_{fb} - \frac{k_B T}{e}\right), \quad (4)$$

where $e = 1.6 \times 10^{-19}$ C, $\varepsilon_0 = 8.86 \times 10^{-12}$ F·m^{-1}, $\varepsilon = 55$ for the (101) facet of anatase TiO_2, and C represents the capacitance. On the basis of this equation, the average donor densities of TiO_2 and NCDs/TiO_2 electrodes are 8.44×10^{18} and 2.67×10^{19} cm^{-3}, respectively. The higher values of the average donor density for NCDs/TiO_2 electrodes are in line with the PEC results. To further investigate the charge-transfer properties of NCDs/TiO_2 composites, the PL lifetime was measured using time-correlated single-photon counting (TCSPC) measurements (Figure 3F). The fast PL decay after decorating the NCDs showed the presence of charge transfer between the NCDs and TiO_2, which suppressed the charge recombination in TiO_2. The hole scavengers could be effectively combined with photogenerated holes and produced electrons in the photocatalyst system, preventing the recombination of charge carriers and leading to a lower PL intensity and shorter PL lifetime. As a result, the efficient charge separation in the NCDs/TiO_2 heterostructure led to the transfer of photogenerated electrons to TiO_2 and the holes to the NCD surface.

4 | CHARGE TRANSFER

In this section, we account for the charge-transfer properties of CDs as either electron donors or acceptors. Doping with metal ions, passivation, and functionalization of surfaces could also improve the charge-transfer properties. This section also introduces the physical principles of the charge transfer of CDs along with representative examples.

After charge excitation and separation, the CDs undergo charge-transfer reactions. CDs can demonstrate superior electron transport properties because they consist of abundant functional groups (hydroxyl, carbonyl, carboxylic, and epoxy groups) on the surface/edge sites and conjugated sp^2/sp^3-hybridized structures.[67,68] It is known that the oxygen-containing functional groups of CDs play an important role in the separation or recombination of electron–hole pairs. In particular, the carboxyl groups act as electron acceptors, forming nonradiative recombination centers. On the contrary, the hydroxyl groups act as electron donors, facilitating fast carrier mobility.[69] In addition, the PL of CDs can be quenched through charge transfer either by electron acceptors (e.g., 2,4-dinitrotoluene and 4-nitrotoluene) or donors (e.g., *N*,*N*-diethylaniline).[1,70] Furthermore, doping with metal atoms can enhance electron-accepting/donating abilities due to the metal ion-to-CD charge-transfer absorption.[26,71] These properties make CDs useful for light and electrical energy conversion applications.

4.1 | Electron donors

Our group has revealed the intrinsic electron donor characteristics of CDs in the synthesis of heterodimeric silver–carbon dot nanoparticles (Ag–CD NPs) using the photoelectron transfer of polysaccharide-derived CDs to Ag^+ ions (Figure 4A,B).[72] Here, CDs act as electron donors to Ag^+ ions that are attracted to the surface of CDs owing to the electrostatic interactions with carboxylic acid groups on the surface. Upon UV irradiation, the CDs were subsequently oxidized from a hydroquinone-like (the combination of sp^2 carbons and hydroxyl groups) structure to a benzoquinone-like structure and served as an electron donor, promoting the reduction of Ag^+ ions on the CD surface. Through the interfacial junction, more electrons pass through the conductive Ag nucleation site and recruit more Ag^+ ions, eventually leading to heterodimeric Ag–CD NPs.

Meanwhile, the electron donor properties of the CDs are strengthened by passivation. Kainth et al.[73] synthesized nitrogen-doped CDs using a series of different nitrogen-rich precursors (such as urea, thiourea, cysteine, and glycine) as passivating agents. The nitrogen-doped CDs exhibited the PL response feature in the presence of picric acid and creatinine. When picric acid was added to the nitrogen-doped CDs, fluorescence quenching occurred due to the interaction of picric acid and nitrogen-doped CDs through acid–base pairing (Figure 4C). Therefore, the

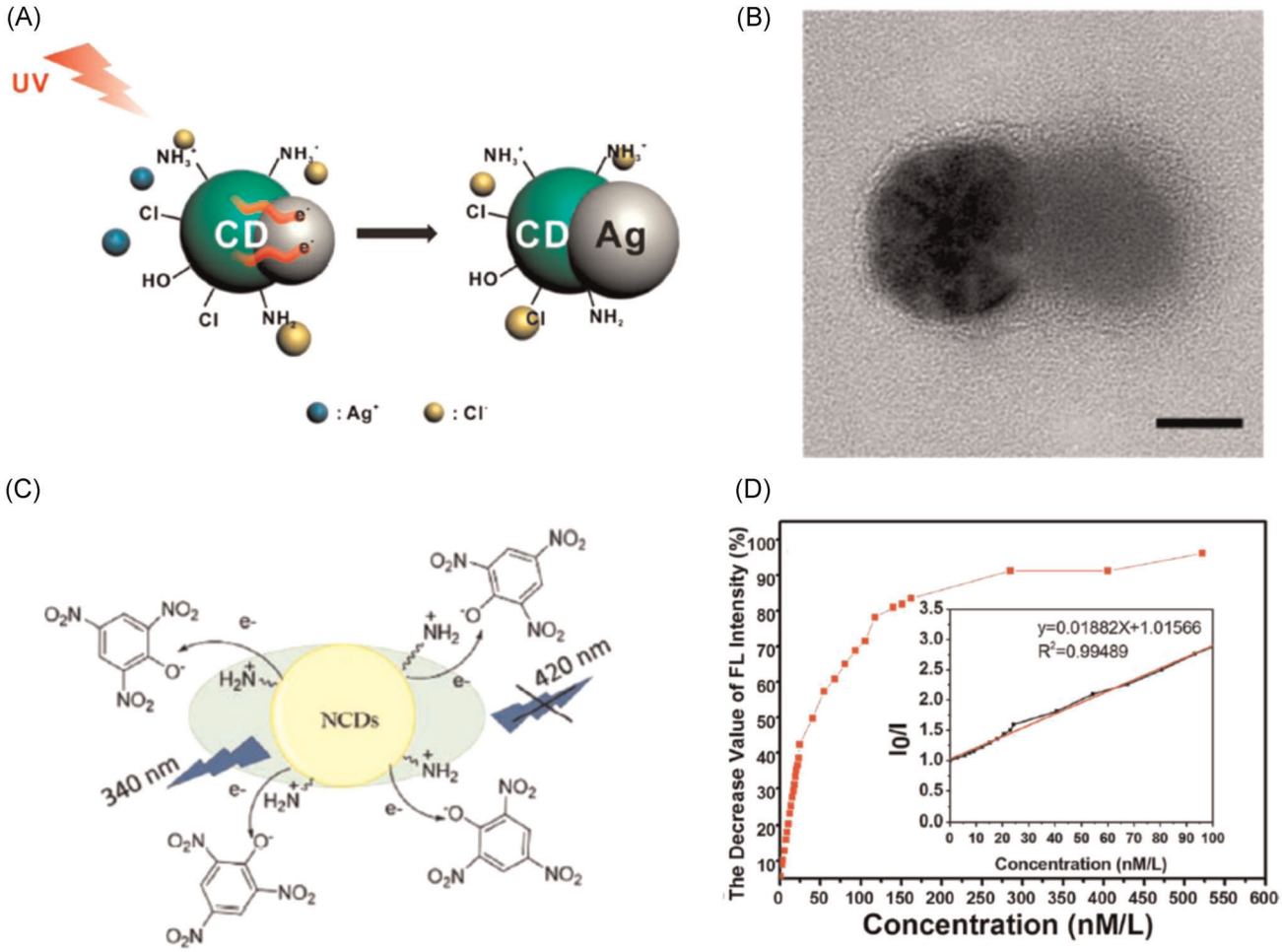

FIGURE 4 (A) Schematic representation of heterodimeric silver–carbon dot nanoparticle (Ag–CD NP) formation. (B) Energy-filtered transmission electron microscopy image of Ag–CD NP (scale bar = 10 nm). Reproduced with permission: Copyright 2014, American Chemical Society.[72] (C) Schematic representation of the fluorescence quenching of nitrogen-doped CD (NCDs). Reproduced with permission: Copyright 2020, The Royal Society of Chemistry.[73] (D) Stern–Volmer relationship between photoluminescence intensity and Fe^{3+} concentration. Reproduced with permission: Copyright 2017, The Royal Society of Chemistry[69]

excited-state electron transfer from electron-rich species on the nitrogen-doped CD surface to the electron-deficient picric acid could take place. Fluorescence restoration was achieved in the presence of creatinine. This phenomenon is closely associated with the strong complexation process between picric acid and creatinine formation in the picric–creatinine complex. Complexation reduced the fluorescence resonance energy transfer phenomenon, thereby enabling fluorescence restoration. On the basis of these properties, Basu and co-workers applied nitrogen-doped CDs as a creatinine-detection probe material. The nitrogen-doped CDs exhibited a maximum PL turn-on response of 50%. Furthermore, PL turn-on/off methodology of nitrogen-doped CDs showed a satisfactory linearity range between 0 and 150 mM, with a detection limit of 0.021 nM for creatinine.

Wang et al.[69] synthesized hydroxyl-functionalized carbon dots (H-CDs) by monoesterification of ethylene glycol (Figure 4D). By increasing the amount of hydroxyl groups, CDs acted as more effective electron donors by facilitating carrier mobility. In particular, H-CDs formed Fe–CD complexes with Fe^{3+} ions through coordination interactions. Throughout the complexation process, electrons were transferred from the excited state of H-CDs to the unfilled Fe^{3+} orbital, leading to nonradiative electron/hole recombination. Therefore, the fluorescence quenching of H-CDs was observed in the presence of Fe^{3+}. Figure 4D shows a decrease in the PL intensities of H-CDs with increasing Fe^{3+} concentration. In addition, the Stern–Volmer quenching curves of the H-CDs demonstrated good linearity with a Stern−Volmer constant (K_{sv}) of $1.91 \times 10^7\ M^{-1}$, indicating dynamic quenching processes.

4.2 | Electron acceptors

The electron-accepting character of CDs has been explored mainly by combining them with electron-donating units such as porphyrins and π-extended tetrathiafulvalene (exTTF). For example, porphyrins have a planar 18-π-electron aromatic structure, which allows efficient pathways for charge transfer through one-electron oxidation of porphyrins and one-electron reduction of CDs.[70] This can be easily observed through the change in absorbance of the Soret band, which is a characteristic of porphyrins. Scharl et al.[68] performed spectrophotometric absorption titration by adding CDs to porphyrin (Figure 5A,B). They observed that, as the quantity of CDs increased, the Soret-band absorption decreased and was slightly red-shifted, resulting in isosbestic points at 420 and 430 nm. Furthermore, the porphyrin-centered fluorescence is quenched, resulting in a Stern–Volmer constant of 0.088 $L \cdot mg^{-1}$.

Unlike porphyrins, exTTF is a pro-aromatic electron donor, because it undergoes a remarkable gain in aromaticity and planarity upon oxidation, forming a stable one-electron oxidized species.[74] As a result of charge transfer through the one-electron redox reaction, a fluorescence quenching of CDs of at least 90% was observed in the presence of exTTF (Figure 5C). Furthermore, according to femtosecond transient absorption (TA) measurements of the CD–exTTF conjugate, 387-nm excitation led to the immediate formation of an excited state with an absorption maximum and minimum at 612 and 438 nm, respectively (Figure 5D). This transient was converted into a new transient within a few picoseconds. The new transient was characterized by a maximum at 463, 549, and 660 nm, as well as a minimum of 423 nm, which corresponds to radiolytic findings regarding the oxidation of exTTF. These results indicate that charge separation, where CDs are one-electron reduced and exTTFs are one-electron oxidized, evolves upon the formation of the initial excited state.

Meanwhile, Lan et al.[75] demonstrated covalently functionalized CDs with 2-(diphenylphosphino)ethylamine (CDs-P). The fluorescence of CDs-P was quenched due to the photo-induced electron transfer mechanism, in which the lone electron pair of the phosphorus atom was transferred to the excited CDs (Figure 5E). The fluorescent peak of CDs-P was blue-shifted from 437 to 430 nm, and the fluorescent quantum yield also decreased from 0.73 to 0.12 (Figure 5F). The excitation spectrum of CD-P also blue-shifted from 345 to 339 nm. Moreover, the calculated fluorescence lifetime of CDs-P decreased from 13.25 to 10.36 ns. Specifically, after the addition of H_2O_2, the charge transfer was interrupted, and CDs-P showed a recovery of fluorescence properties with an increase in the fluorescence lifetime to 11.29 ns. This indicates that CDs-P could be employed as a sensor probe with a high sensitivity to H_2O_2.

5 | SOLAR-TO-ENERGY CONVERSION APPLICATIONS

In this section, based on the superior photophysical and photochemical properties of CDs discussed thus far, we present the representative examples of CDs used in the photovoltaic and photocatalytic systems. In particular, we summarize the multifaceted roles of CDs in the solar-to-energy conversion systems.

5.1 | Photovoltaic cells

CDs have a large surface area, strong light absorption, and excellent electrical properties, indicating their potential for applications in a variety of photovoltaic cells. Furthermore, CDs can generate electron–hole pairs and suppress electron–hole pair recombination. The abundant functional groups on the surface make CDs an excellent electron donor/acceptor. Therefore, CDs are promising candidates for photovoltaic cells and can replace expensive and toxic semiconducting nanoparticles.

The following studies have reported that CDs can act as light absorbers (e.g., sensitizers) in solid-state devices. Briscoe et al.[76] prepared three biomass-derived (glucose, chitin, and chitosan) CDs and demonstrated that the performance of photovoltaic cells was significantly dependent upon the surface functionalities. Owing to different functional groups according to precursors, the resultant CDs varied in their surface characteristics and light absorption abilities. The photovoltaic performances of the three CDs were enhanced within a ZnO nanorod-based device, compared with an uncoated device. However, a strong correlation between the light absorption features and the resulting photocurrent was not observed. Specifically, the thicker layer consisting of glucose-derived CDs enabled a higher light absorption but limited the photocarrier collection due to recombination. Conversely, the lower coating density of chitin-derived CDs was not sufficient to reduce recombination, leading to a low shunt resistance. The chitosan-derived CDs produced the highest device performance, with a power conversion efficiency (PCE) of 0.061%. The results indicated that the surface functionalities of CDs determine the degree of surface interactions between CDs and ZnO nanorods, affecting the extent of charge transfer within the sensitizer layer. In other words, the device performance is affected by the structural characteristics of the CD layer rather than the individual light-harvesting capabilities.

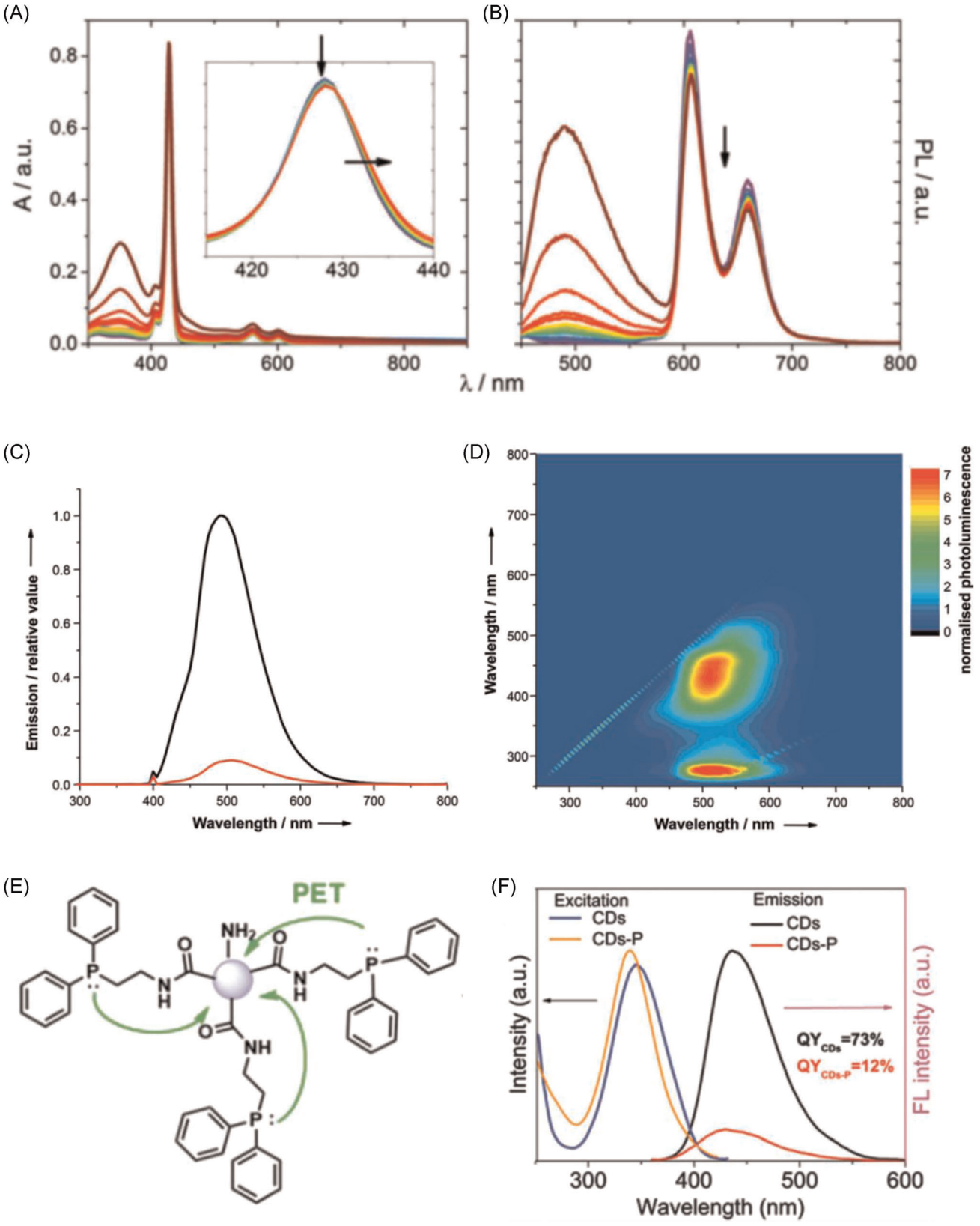

FIGURE 5 (A) Absorption and (B) fluorescence ($\lambda_{ex} = 420$ nm) spectra of porphyrins throughout a titration with carbon dots (CDs) (blue to dark red). Reproduced with permission: Copyright 2018, The Royal Society of Chemistry.[68] (C) Steady-state emission spectra ($\lambda_{ex} = 400$ nm) of CDs (black) and CD−exTTF conjugate (red). (D) Excitation and emission 3D map of CD−exTTF conjugate obtained at 295 K in dimethyl sulfoxide. Reproduced with permission: Copyright 2018, Wiley.[74] (E) Schematic of the electron transfer mechanism of 2-(diphenylphosphino)ethylamine (CDs-P). (F) Fluorescence excitation and emission spectra ($\lambda_{ex} = 350$ nm) of CDs and CDs-P. Reproduced with permission: Copyright 2015, The Royal Society of Chemistry[75]

Our group fabricated CD-supported silver nanoparticles (CD–Ag nanoparticles), where CDs served as a reducing agent and template (Figure 6A).[22] When incorporating the CD–Ag nanoparticles into the active layer, the PCE of PTB7:$PC_{71}BM$-based polymer solar cells (PSCs) was enhanced from 7.53% to 8.31% due to the broad light absorption by the surface plasmon resonance of the CD–Ag nanoparticles (Figure 6B). In addition, the plasmonic CD–Ag nanoparticles produced a high internal quantum efficiency (99%), indicating that all absorbed photons generate separated charge carriers, and the photogenerated carriers are collected into the electrodes without any loss.

The efficient electron transport layer (ETL) plays a key role in promoting the charge carrier separation and electron extraction in photovoltaic cells. The ETL mainly consists of metal oxides, including SnO_2,[78–80] TiO_2,[4,81–83] and ZnO.[84,85] In recent years, CDs have been used to modify the ETL for boosting electron extraction.[78] For example, the incorporation of CDs into the SnO_2-based ETL significantly enhanced the PCE of perovskite solar cells from 19.15% to 22.77% and increased the long-term device stability against humidity. These significant achievements are attributed to the dramatically increased electron mobility of the modified ETL, thereby inducing the traps/defects passivation of the interface between the ETL and perovskite and promoting the formation of highly crystallized perovskite. This study demonstrated that CDs could serve as excellent additives for producing efficient ETLs in perovskite-based optoelectronics. CDs were incorporated into the electron extraction layer, facilitating more efficient charge transfer. Zhu et al.[4] deposited a layer of CDs between the perovskite sensitizer and the TiO_2 film as a charge-transfer bridge, thereby promoting efficient electron injection from the perovskite to the TiO_2 nanoparticles without capturing any electrons. By introducing CDs as an electron extraction layer, the PCE was improved from 8.81% to 10.15%. The role of CDs as electron acceptors was confirmed by the PL quenching measurements, which showed dramatic PL quenching of the perovskite and higher internal quantum efficiencies. The femtosecond TA spectroscopy further demonstrated that the electron extraction time decreased from 260–307 to 90–106 ps in the presence of CDs (Figure 6C,D). The results indicated that CDs could act as a superfast electron funnel due to the widely distributed π orbitals, thereby enhancing the electronic coupling between the perovskite sensitizer and TiO_2 nanoparticles.

Gao et al.[77] incorporated CDs synthesized from graphene oxide between the Si and Au electrode to serve as an efficient hole transport/electron blocking layer that suppresses anodic carrier recombination (Figure 6E). The termination group of Si was first optimized by H-, SiO_x-, and CH_3 surface functionalities, because the non-passivated Si has many dangling surface bonds that induce carrier recombination. Methylated Si exhibited the highest photovoltaic performance owing to the reduced interfacial recombination. The CDs incorporated in the device drastically improved the photovoltaic parameters and PCE, compared with the devices using only Au electrode or graphene oxide substituted for CDs. In addition, the dark current within the CDs incorporated in the device decreased, which highlights the reduced electron leakage that could induce anodic charge recombination (Figure 6F). The photovoltaic performances of the CD-based devices were enhanced by the strong electric field at the Si/CD heterojunction, thereby leading to an efficient charge carrier separation. The appropriate alignment between the LUMO of CDs and the CB of Si ensured low interfacial recombination, which highlights the ability of CDs as an effective hole transport/electron blocking layer.

The Giberti group incorporated CDs as a work function modifier into the poly(ethylene imine) (PEI) layer to increase the exciton dissociation probability in photovoltaic cells.[86] The net photocurrent density as a function of effective voltage revealed that the devices with the CD-doped PEI layer exhibited a much higher charge separation efficiency, compared with the devices with the pristine PEI layer. Furthermore, impedance spectroscopy showed a significantly reduced series resistance in a PSC with a CD-doped PEI layer. The Kelvin probe force microscopy clearly showed that the work function of ITO with the CD-doped PEI layer was higher than that of the ITO with the pristine PEI layer, inducing a stronger internal field. The internal field induced by the work function difference between the anode and cathode can influence the exciton dissociation probability. The PCE with the CD-doped PEI layer exhibited an average PCE of 9.37%, which is higher than that of the pristine PEI layer. Consequently, the improvement in the PCE performance is attributed to the enhanced electron transport properties due to the exciton extraction properties by CD doping (Tables 1–3).

5.2 | Photocatalysts

Photocatalysis requires efficient coupling of light harvesting and charge transfer in catalytic processes, and CDs have been proposed as potential sensitizers or direct photocatalysts in the process of solar energy conversion. CDs have

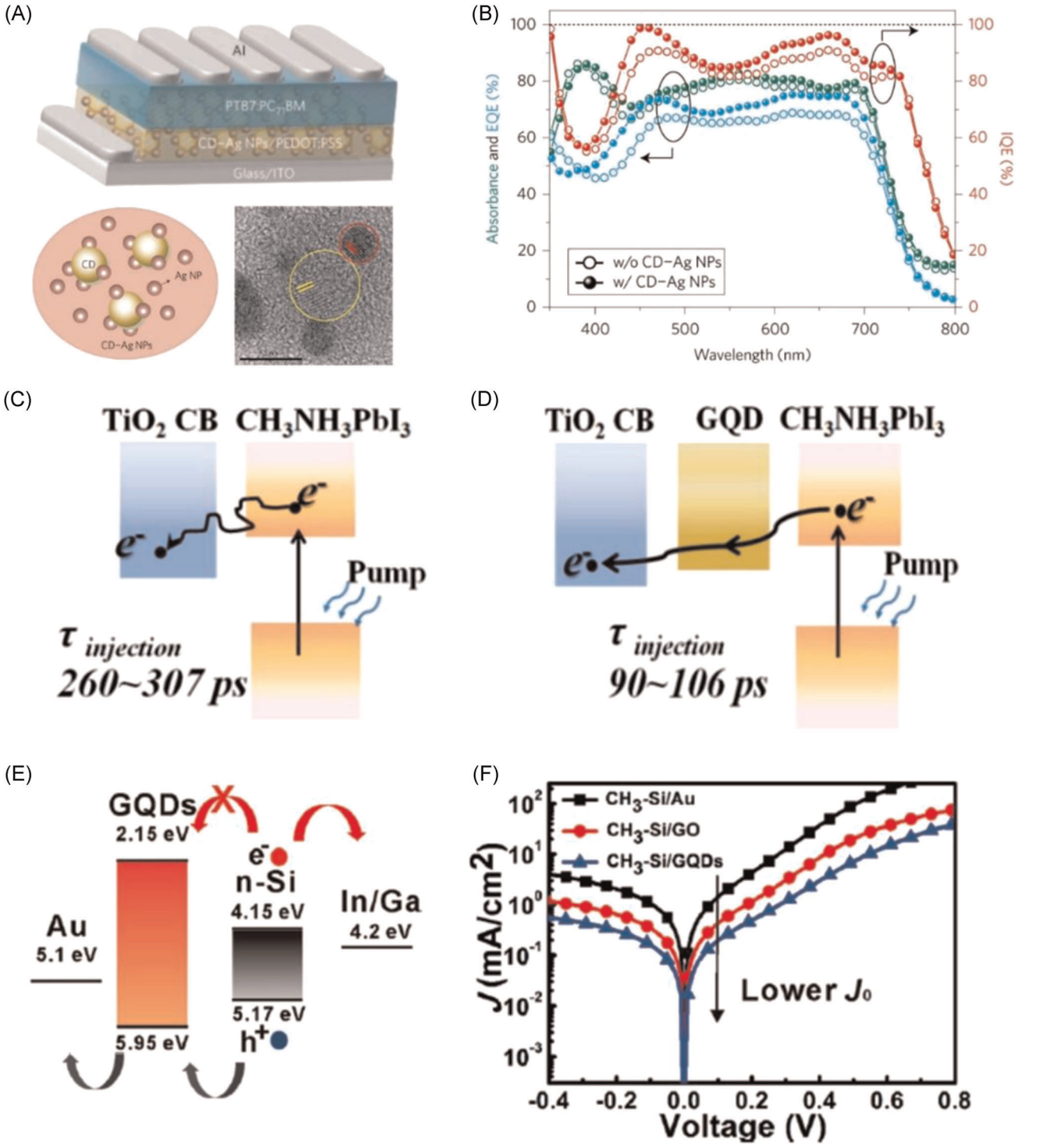

FIGURE 6 (A) Device structure of PTB7:$PC_{71}BM$-based polymer solar cells (PSCs) with and without CD–Ag nanoparticles. Schematic illustration and transmission electron microscopy image of CD–Ag nanoparticles. Reproduced with permission: Copyright 2013, Springer Nature.[22] (B) Internal quantum efficiency (IQE) (red), external quantum efficiency (EQE) (blue), and total absorption (green) of PSCs with CD–Ag nanoparticles. The filled and open circles represent device parameters with and without CD–Ag nanoparticles, respectively. Reproduced with permission: Copyright 2013, Springer Nature.[22] (C, D) Schematic representation of electron generation and extraction, and injection lifetime of perovskite solar cells (C) without and (D) with graphene quantum dot (GQD) layer. Reproduced with permission: Copyright 2014, American Chemical Society.[4] (E) Energy band diagrams of CH_3—Si/GQDs heterojunction device. Reproduced with permission: Copyright 2014, American Chemical Society.[77] (F) *J*–*V* curves of CH_3—Si/Au, CH_3—Si/GO, and CH_3—Si/GQDs solar cells under dark condition. Reproduced with permission: Copyright 2014, American Chemical Society[77]

TABLE 1 Representative examples of CDs for photovoltaic cells

Precursors	Synthetic methods	Role of CDs	PCE (w/o CDs) (%)	PCE (w/CDs) (%)	References
Biomass precursors (chitin, chitosan, D(+)-glucose)	Hydrothermal reaction	Photosensitizer	0.0004	0.077	Briscoe et al.[76]
Graphene oxide	Acid oxidation and hydrothermal reaction	Photosensitizer and charge extraction	6.70	7.60	Kim et al.[87]
Carbon fiber	Hydrothermal reaction	Photosensitizer and charge extraction	7.52	8.34	Kim et al.[88]
Graphene oxide	Solvothermal reaction	Electron extraction	8.80	10.00	Moon et al.[84]
Graphite rod	Electrochemical reaction	Electron extraction and transport	8.81	10.15	Zhu et al.[4]
L-Cystine, *O*-phenylenediamine	Solvothermal reaction	Electron extraction	19.15	22.77	Hui et al.[78]
Citric acid and urea	Microwave-assisted reaction	Hole extraction and transfer	5.93	7.22	Zhang et al.[83]
Citric acid and urea	Solvothermal reaction	Hole extraction and transfer	14.70	16.20	Benetti et al.[89]
Graphene sheets	Hydrothermal reaction	Hole transport/electron blocking layer	2.92	6.63	Gao et al.[77]
Neutral red powder, ethylenediamine	Microwave-assisted reaction	Work function modifier	1.06	9.37	Park et al.[86]

Abbreviations: CD, carbon dot; PCE, power conversion efficiency.

notable advantages such as high chemical stability, strong and broad light absorption, excellent electron and hole transport ability, and nontoxicity, making them promising candidates for photocatalytic applications. CDs can act not only as individual photocatalysts, but also as multifunctional components of complex photocatalysts, providing a wider light response, promoting the separation of e^-/h^+ pairs, and stabilizing the complex photocatalyst.[25,111,112]

The intrinsic photocatalytic characteristics of the CDs were revealed by the Teng group who fabricated N-doped CDs (NCDs) consisting of p- and n-type domains for photocatalytic water splitting (Figure 7A).[90] The developed NCD photocatalyst exhibited p-type conductivity by oxygen-bearing functional groups on the surface and n-type conductivity by an inserted nitrogen atom. According to the Mott–Schottky analysis, NCDs indicated straight lines with negative and positive slopes, supporting the coexistence of p-type and n-type conductivities. The coexistence of p- and n-domains in the NCDs could build photochemical diodes to facilitate charge separation. In addition, NCDs showed CB minimum and VB maximum values of approximately −0.85 and 1.35 eV (vs. Ag/AgCl), respectively. The band gap energy of NCDs (2.2 eV) includes the energy levels for water reduction and oxidation, suggesting that NCDs can catalyze overall water splitting under visible-light irradiation. When water splitting was carried out for 27 h by applying external visible light with the NCD catalyst, the ratio of H_2 and O_2 production was maintained at almost 2:1.

CDs can efficiently enhance photocatalytic activity by forming a complex with other components used in photocatalysts such as metals and semiconductors. CDs can play a role in effectively improving the photo-induced charge separation in complex photocatalytic systems and enhancing light absorption and photocatalytic activity owing to their unique photoelectric properties. As a representative example, our group reported the self-assembly of the alginate-based CD and cobalt polyoxometalate (Co-POM), resulting in the synthesis of the spherical hybrid of CD/Co-POM for visible light-driven water oxidation (Figure 7B).[91] The HOMO level of the CDs was 7.78 eV (vs. RHE), and this was more positive compared with the thermodynamic redox potential for water oxidation, 1.23 V (vs. RHE), and the onset potential for water oxidation by Co-POM, 1.769 V (vs. RHE). Thus, the HOMO level of CDs can provide an optimal band gap and band-edge position for effective water oxidation reactions. Owing to the shortcut transfer of photogenerated holes under visible-light irradiation, the CD/Co-POM hybrid provides a rapid scavenging of holes and collection of a long-lived oxidation state of Co-POM for efficient solar water oxidation. The reduction in PL intensity and PL lifetime supports the efficient transfer of charge carriers from CD to Co-POM. The PL intensity of CD/Co-POM reduced by 72%, compared with that of the CD, and the PL lifetime decreased from 4.12 ns in CD to 1.77 ns in CD/Co-POM. As a result, the CD/Co-POM hybrid exhibited a high turnover number of 552 for oxygen generation, achieving an excellent performance in the photocatalytic oxygen evolution.

Achilleos et al.[92] employed CDs as light absorbers, along with a nickel (Ni) bis(disphosphine) H_2 evolution cocatalyst (NiP) for the conversion of biomass into renewable H_2 and organics (Figure 7C). The CDs exhibit two characteristics for efficient photocatalysis: (i) the presence of both oxidative and reductive quenching mechanisms, and (ii) slow bimolecular recombination and higher yields of long-lived carriers. To understand the electron transfer dynamics between CDs and NiP, TA spectroscopy in the femtosecond–nanosecond (fs-TA) and microsecond–second (μs-TA) regimes was employed. According to the fs-TA spectrum (355-nm excitation), the CDs showed broad absorption properties in the visible region. When ethylenediamine tetraacetic acid (EDTA) was added as a sacrificial electron donor, the absorption decayed faster by approximately twice the original value, with the decay half-life increasing from 20 to 40 ps, because the light-induced h^+ was scavenged by EDTA. Furthermore, when NiP was added as an electron scavenger, quenching of the electron signal (~0.5 ms) was induced, and a negative signal was assigned to the ground-state bleach of NiP, as its reduction by CDs was observed at 500 nm. This indicates a direct electron transfer from CDs* to NiP, reflecting oxidative quenching. Meanwhile, the addition of EDTA caused prolonged electron signals at 700 nm, demonstrating that reductive quenching depends on the differences in the energy of trapped charges. In addition, the bimolecular recombination lifetime of CD is approximately 45 ps, and the proportion of long-lived carriers is approximately 15%–20%. On the basis of these results, CDs can be considered as excellent photocatalysts for photoreforming.

Li et al.[98] fabricated a Ru@CD photocatalyst for hydrogen evolution reaction (HER). The collaborative effect between the CDs and Ru nanoparticles facilitated the adsorption and dissociation of H_2O molecules. As the electrons transfer from H_2O through Ru to the C atom of CDs, charge density redistribution is induced, leading to electron-abundant CDs and a hole-abundant Ru cluster. Therefore, the polarized Ru cluster adsorbed on the CDs acts as a charge donor to enhance the Ru–O interaction, facilitating the dissociation of H_2O. Meanwhile, dissociated H atoms were captured by the Ru–H interaction, thereby promoting H_2 generation. Owing to these characteristics, Ru@CDs can be applied as promising HER catalysts. In particular, Ru@CD that was annealed at 480°C (named as $Ru@CD_{480}$) exhibited the highest HER activity (Figure 7D). $Ru@CD_{480}$ showed a low overpotential of

TABLE 2 Representative examples of CDs as photocatalysts

Materials	Role of CDs	Catalytic application	Catalytic efficiency	References
N-doped CDs	Electron donor	Overall water splitting	2.2 eV (band gap)	Yeh et al.[90]
CD/Co-POM (cobalt polyoxometalate) hybrid	Electron donor	OER	552 (TON)	Choi et al.[91]
CD/NiP (nickel bis(diphosphine)	Electron donor	HER	45 ps (recombination lifetime)	Achilleos et al.[92]
CD-NiP	Electron donor	HER	1094 ± 61 (TON)	Martindale et al.[93]
N-doped CDs@TiO_2	Electron donor	Photodegradation of organic pollutant	Complete degradation after 80 min	Mas et al.[94]
N-doped CDs	Electron donor	CO_2RR	198 mV·dec^{-1} (Tafel slope), 100 mA·cm^{-2} (J)	Wu et al.[95]
B-doped CDs	Electron donor	ORR	4.2 mA·cm^{-2} (J_L), −0.05 V (onset potential), −0.26 V ($E_{1/2}$), 3.81 (n)	Van Tam et al.[96]
N-doped CDs	Electron donor	Photochemical radical perfluoroalkylation	82% yield	Rosso et al.[97]
Ru@CDs	Electron acceptor	HER	10 mA·cm^{-2} (η), 47 mV·dec^{-1} (Tafel slope), 0.80 mA·cm^{-2} (J), 6.35 Ω (R_{ct})	Li et al.[98]
N-CDs (nitrogen-doped CDs)/g-C_3N_4 (graphitic carbon nitride)	Electron acceptor	HER	13.30 μmol·g^{-1}·h^{-1} (photocatalytic hydrogen evolution rate)	Zou et al.[99]
Cu–N-doped CDs	Electron donor and acceptor	Photooxidation of 1,4-DHP (1,4-dihydro-2,6-dimethylpyridine-3,5-dicarboxylate)	171.8 μs·cm^{-1} (σ)	Wu et al.[71]
NH_2-MIL-88B(Fe)/CDs composite	Electron donor and acceptor	Photoreduction of Cr(VI) and photodegradation of methylene blue	95% (Cr(VI) reduction efficiency), 0.05491 min^{-1} (reaction rate of Cr(VI) reduction) 92% (methylene blue degradation efficiency), 0.0220 min^{-1} (reaction rate of methylene blue degradation)	Shao et al.[100]
ZnCu-CDs	Electron donor and acceptor	Photooxidation of 1,4-dihydro-2,6-dimethylpyridine-3,5-dicarbonate (DHP)	93.9% (conversion of 1,4-DHP), 0.03 min^{-1} (photooxidation reaction rate)	Wu et al.[101]
Co_3O_4–CDs–C_3N_4	Electron donor and acceptor	HER and CO_2RR	0.17 V (η), ~95% (total Faradaic efficiencies of CO and H_2)	Guo et al.[102]

Abbreviations: CO_2RR, CO_2 reduction reaction; $E_{1/2}$, half-wave potential; HER, hydrogen evolution reaction; J, current density; J_L, limiting current density; n, electron transfer number; OER, oxygen evolution reaction; ORR, oxygen reduction reaction; R_{ct}, charge-transfer resistance; TON, turnover number; η, overpotential; σ, electric conductivity.

TABLE 3 Representative examples of CDs for photoelectrocatalysts

Materials	Role of CDs	Catalytic application	Catalytic efficiency	References
NCDs/WO_3	Electron donor	PEC water oxidation	1.42 mA·cm^{-2} (J_{ph})	Kong et al.[63]
NiOOH/FeOOH/CDs/$BiVO_4$ photoanode	Electron donor	PEC water splitting	5.99 mA·cm^{-2} (J_{ph}), 2.29% (PCE)	Ye et al.[103]
CD–TiO_2 nanotube heterojunction films	Electron donor	Degradation of methylene blue	0.023 min^{-1}	Pan et al.[104]
CDs/WO_3 composites	Electron donor	PEC solar energy conversion	1.46 mA·cm^{-2} (J_{ph})	Shi et al.[105]
CDs/CuSCN composite	Electron acceptor	Hole-transporting p-type thin films	0.082 V (onset potential), 17.4 kΩ (R_{ct})	Wang et al.[106]
NCDs/np^+-Si (n-type silicon)	Electron acceptor	HER	0.21 V (onset potential), 34.7 mA·cm^{-2} (J_{ph})	Chen et al.[107]
Cu_2S/CDs	Electron acceptor	PEC water splitting	1.05 mA·cm^{-2} (J_{ph}), 90.9% (stability), 70.1 Ω·cm^2 (R_{ct})	Li et al.[108]
CD/g-C_3N_4 (graphitic carbon nitride) composites	Electron acceptor	PEC degradation of organic pollutants	97.2% (methylene blue degradation), 51.6% (phenol degradation)	Zhang et al.[109]
Ru@CDs	Electron acceptor	HER	0 mV (η), 47 mV·dec^{-1} (Tafel slope)	Li et al.[98]
CD/Co_3O_4–Fe_2O_3	Electron acceptor	Water oxidation	1.48 mA·cm^{-2} (J_{ph}), 0.20% (PCE), 230 ± 37 Ω (R_{ct})	Zhang et al.[110]

Abbreviations: CD, carbon dot; HER, hydrogen evolution reaction; J_{ph}, photocurrent density; NCD, N-doped carbon dot; PCE, photon-to-current efficiency; PEC, photoelectrochemical; R_{ct}, charge-transfer resistance; η, overpotential.

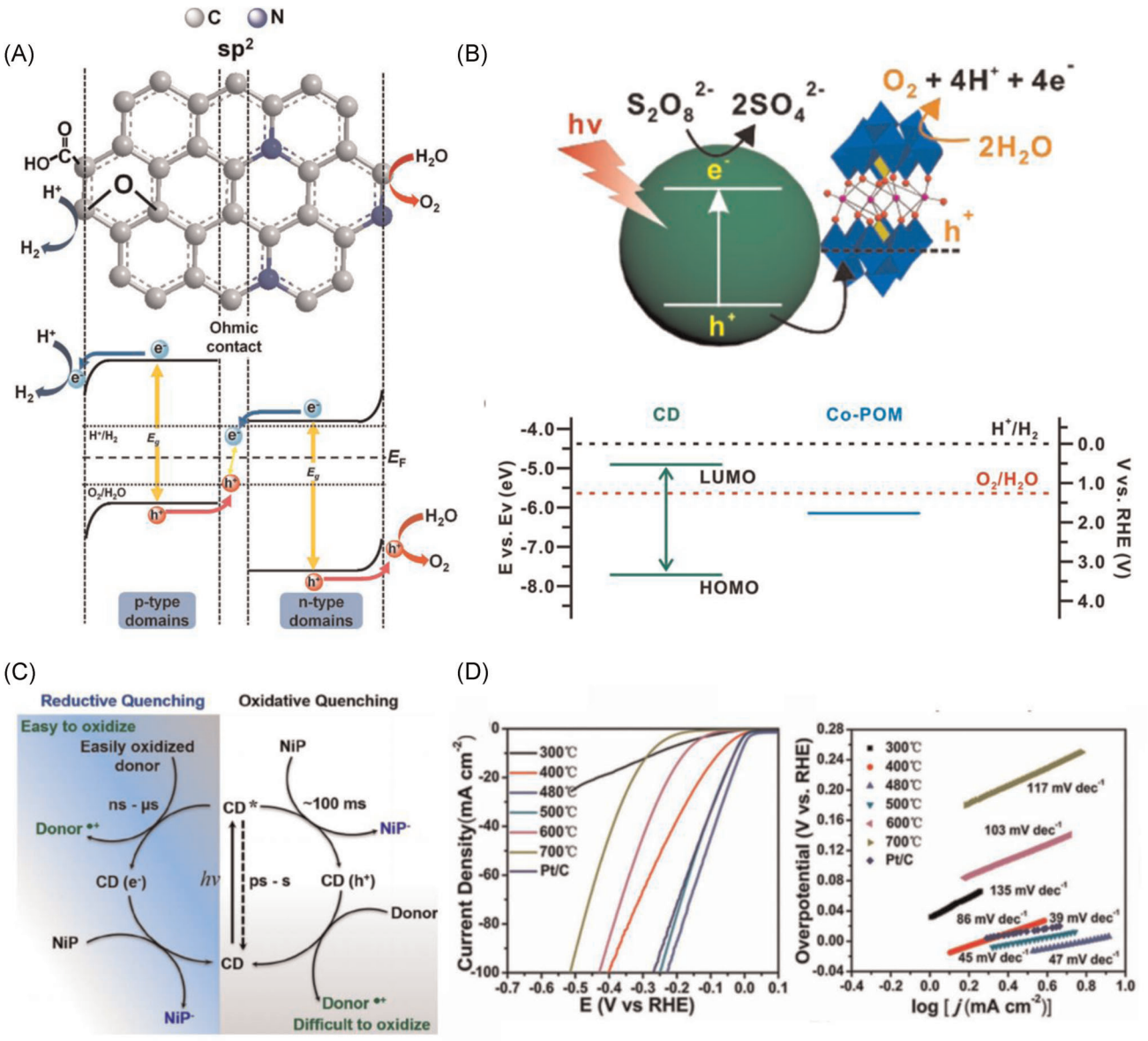

FIGURE 7 (A) Schematic illustration of the configuration and energy diagram of N-doped CDs. Reproduced with permission: Copyright 2014, Wiley.[90] (B) Schematics of photoelectron transfer reaction and band diagram of CD and Co-POM (cobalt polyoxometalate). Reproduced with permission: Copyright 2018, American Chemical Society.[91] (C) Feasible charge-transfer reactions of CDs with NiP (Ni bis (disphosphine)). Reproduced with permission: Copyright 2020, Wiley.[92] (D) HER polarization curves and Tafel plots of Ru@CDs annealed at different temperatures and Pt/C catalyst as the control group. Reproduced with permission: Copyright 2018, Wiley.[98] CD, carbon dot; HER, hydrogen evolution reaction; HOMO, highest occupied molecular orbital; LUMO, lowest unoccupied molecular orbital

10 mV and a Tafel slope of approximately 47 mV·dec^{-1}, which is superior to that of a commercial Pt/C catalyst (39 mV·dec^{-1}). In addition, Ru@CD$_{480}$ showed an excellent exchange current density of 0.80 mA·cm^{-2} and charge-transfer resistance (R_{ct}) of 6.35 Ω, which is approximately twice as low as that of the commercial Pt/C catalyst (39 mV·dec^{-1}). These results indicate that Ru@CD$_{480}$ possesses excellent charge-transfer capacity and fast interfacial electronic transfer kinetics during HER due to the synergistic effect between the Ru nanoparticles and CDs.

5.3 | Photoelectrocatalysts

CDs can significantly improve PEC properties due to the quantum size effect, broadband optical absorption, high electrical conductivity, and analogous semiconductor properties. Moreover, numerous studies have indicated that the electron-donating and electron-accepting properties of CDs may be advantageous for guiding the flow of photogenerated charges. Therefore, with these characteristics, CDs can be considered as excellent candidates as sensitizers to enhance the solar absorption of the host

materials in PEC cells.[25,106,107] According to recent studies, CDs have been coupled with semiconductor nanoparticles such as Cu_2O, TiO_2, $BiVO_4$, g-C_3N_4, and Cu_2S to improve their PEC performance.[109]

In particular, due to the electron affinity of N, it is known that N-doped CDs exhibit a promising potential in enhancing PEC performance by increasing the active sites and effectively improving the charge-transfer rate. As a representative example, Kong et al.[63] fabricated a WO_3 nanoflake photoanode that was N-doped and CDs-modified (NCDs/WO_3) for PEC water oxidation. NCDs/WO_3 exhibit an excellent photocurrent density of 1.42 mA·cm^{-2} (at 1.0 V vs. saturated calomel electrode) in 1 M H_2SO_4 solution and a negative shift of 70 mV in the onset potential, compared with bare WO_3. The mechanism of the enhanced PEC activity of NCDs/WO_3 is explained based on the movement of the photogenerated holes and electrons, which occurs because the LUMO of NCDs is more positive than that of WO_3 (Figure 8A). The photogenerated holes from the VB of WO_3 can be transferred to the HOMO of N-doped CDs. Moreover, the photogenerated electrons can transfer from the N-doped CDs to WO_3. Furthermore, owing to the built-in electron field, the photogenerated electrons and holes are effectively separated.

In contrast to the previous example, there is another example where CDs act as electron acceptors. Wang et al.[106] fabricated a CD/CuSCN composite thin film through the decoration of CuSCN nanorod thin films with CDs. The hybridization of CDs did not change the nanorod structure and p-type properties of the CuSCN thin film, and the VB potential of CDs/CuSCN (0.20 V) was more negative than that of the CuSCN thin film (0.10 V), facilitating charge separation in PEC applications. Figure 8B shows a schematic diagram of the efficient charge transfer and separation processes occurring within the CD/CuSCN thin-film electrode. Upon light irradiation, the CD/CuSCN thin film can be excited to generate electron–hole pairs. In addition, when CDs were decorated on the surface of the CuSCN thin film, a heterojunction could be developed at the interface between the CDs and CuSCN nanorods. This facilitates the separation of photogenerated electron–hole pairs, and photogenerated electrons can be efficiently transferred from the CB of CuSCN to the CD surface. Consequently, the photocurrent of the CD/CuSCN thin film significantly improved by approximately 6.5 times, compared with that of the pristine CuSCN thin film.

Ye et al.[103] fabricated a NiOOH/FeOOH/CDs/$BiVO_4$ (NFCB) photoanode for PEC water splitting by embedding CDs between the $BiVO_4$ core and NiOOH/FeOOH shell. As shown in Figure 8C, when the NFCB photoanode was irradiated with visible light, photogenerated electrons and holes were generated by CDs and $BiVO_4$. In this system, CDs act as photosensitizers that extend the light-harvesting range of the $BiVO_4$ electrode from UV to near infrared, thus increasing the light absorption and separation of electrons and holes. At the same time, CDs improved the hole transport ability by reducing the conductivity of FeOOH, which functioned as a hole transport layer. In other words, CDs accelerated the oxygen evolution reaction kinetics by maintaining efficient hole transfer from $BiVO_4$ to the NiOOH/FeOOH layer. As a result, the NFCB photoanode demonstrated a noticeable photocurrent density of 5.99 mA·cm^{-2} at 1.23 V (vs. RHE) and a high applied bias photon-to-current efficiency of 2.29% at 0.6 V (vs. RHE).

Zhang et al.[109] synthesized a CDs/g-C_3N_4 (graphitic carbon nitride) photoanode for the degradation of organic pollutants (methylene blue and phenol). The introduction of CDs to g-C_3N_4 photoelectrodes effectively separated the e^-–h^+ pairs and electron transfer from g-C_3N_4 to the CDs. Thus, the electrons emitted from the CB of g-C_3N_4 could be trapped by CDs. Therefore, the CDs could react with molecular oxygen to produce superoxide anion radicals, which oxidized pollutants. Consequently, the CDs/g-C_3N_4 photoelectrodes demonstrated a superior degradation efficiency of 97.2% (Figure 8D), indicating that the synergistic effect of the bias potential and illumination enhances the separation of the electron–hole pairs. Meanwhile, as shown in Figure 8D, temporal changes in the absorption of methylene blue solutions under visible light were observed in the presence of CDs/g-C_3N_4. This result implies the destruction of the molecular structure of methylene blue. Furthermore, CDs/g-C_3N_4 showed a longer electron lifetime (61.2 ms) than that of g-C_3N_4 (10.8 ms). This result suggests an improved charge recombination of CDs/g-C_3N_4. The CDs/g-C_3N_4 photoelectrodes exhibited a remarkable durability and stability. The CDs/g-C_3N_4 showed only a slight decrease in efficiency from 97.2% to 85.4% after five cycles.

6 | SUMMARY AND OUTLOOK

In this review, we present the recent research progress on various CD-based photoactive nanocomposites and their semiconducting features as charge carriers for solar-to-energy conversion applications. In particular, this review has focused on a stepwise mechanism that modulates the photoexcited charge carriers of CD-based materials from generation to separation and transfer to overcome the intrinsically low performance of CDs for applications in practical photovoltaic cells and photocatalysts. Although the separation efficiency and

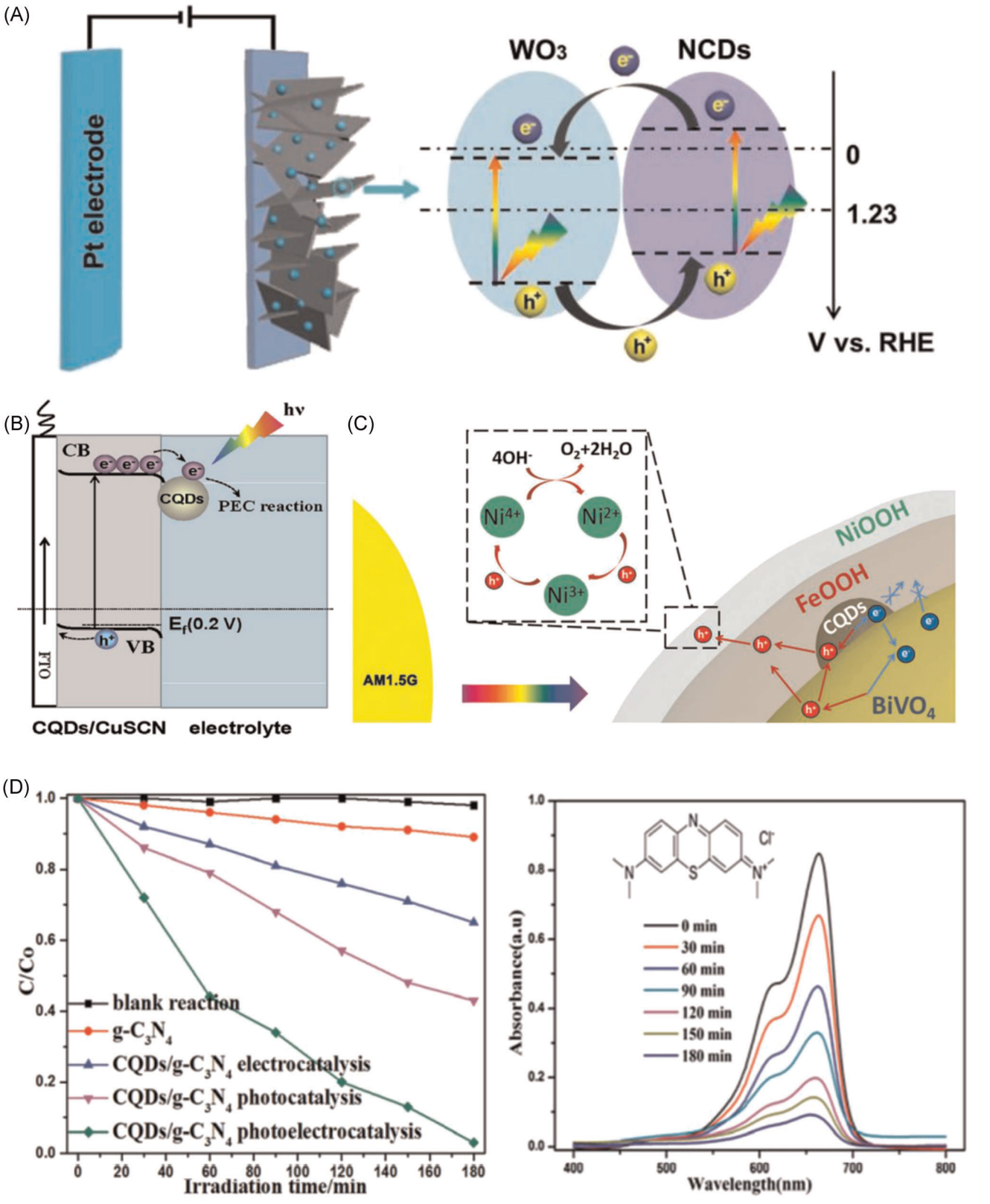

FIGURE 8 (A) Schematic illustration of the N-doped, carbon dots-modified WO_3 nanoflake (NCDs/WO_3) photoanode. Reproduced with permission: Copyright 2018, Wiley.[63] (B) The diagram illustration of charge transfer and separation process within the fabricated CDs/CuSCN composite thin-film electrode. Reproduced with permission: Copyright 2017, Elsevier.[106] (C) Schematic representation of the mechanism of photoelectrochemical water oxidation at the NiOOH/FeOOH/CDs/$BiVO_4$ (NFCB) photoanode. Reproduced with permission: Copyright 2017, The Royal Society of Chemistry.[103] (D) The degradation of methylene blue over the g-C_3N_4 (graphitic carbon nitride) and CDs/g-C_3N_4 photoanodes and absorption spectra under visible-light irradiation of the methylene blue solution in the presence of the CDs/g-C_3N_4 photoanodes. Reproduced with permission: Copyright 2017, The Royal Society of Chemistry[109]

transfer kinetics of CDs are generally lower than those of inorganic-based semiconductors, CDs have been considered as efficient energy converters that prevent the recombination of photoexcited electron–hole pairs and facilitate the transfer of charge carriers effectively by (i) varying chemical functional groups and sp^2/sp^3 domains on the CD surface, (ii) controlling the surface charge distribution induced by heteroatom doping, and (iii) hybridizing nanocomposite assembly with other nanomaterials, enabling the adjustment of suitable energy band structures. As the optical properties and photoactivities of CDs are highly controllable and processable with various synthetic protocols, we anticipate that versatile CDs can serve as a promising alternative for environment-friendly solar-to-energy and fuel conversion systems, as well as expand their applications in future advanced optoelectronics and energy-harvesting devices.

ACKNOWLEDGMENTS

This study was supported by the National Research Foundation of Korea (NRF-2018R1A5A1025208 and NRF-2017M3A7B4052802).

ORCID

Namhee Kim https://orcid.org/0000-0003-2214-5588
Jiyoung Lee https://orcid.org/0000-0002-6009-7524
Minsu Gu http://orcid.org/0000-0002-6270-7496
Byeong-Su Kim http://orcid.org/0000-0002-6419-3054

REFERENCES

1. Wang X, Cao L, Lu F, et al. Photoinduced electron transfers with carbon dots. *Chem Commun*. 2009:3774-3776.
2. Sun Y-P, Zhou B, Lin Y, et al. Quantum-sized carbon dots for bright and colorful photoluminescence. *J Am Chem Soc*. 2006;128:7756-7757.
3. LeCroy GE, Sonkar SK, Yang F, et al. Toward structurally defined carbon dots as ultracompact fluorescent probes. *ACS Nano*. 2014;8:4522-4529.
4. Zhu Z, Ma J, Wang Z, et al. Efficiency enhancement of perovskite solar cells through fast electron extraction: the role of graphene quantum dots. *J Am Chem Soc*. 2014;136:3760-3763.
5. Das SK, Liu Y, Yeom S, Kim DY, Richards CI. Single-particle fluorescence intensity fluctuations of carbon nanodots. *Nano Lett*. 2014;14:620-625.
6. Liu Y, Kim DY. Ultraviolet and blue emitting graphene quantum dots synthesized from carbon nano-onions and their comparison for metal ion sensing. *Chem Commun*. 2015;51:4176-4179.
7. Cao L, Wang X, Meziani MJ, et al. Carbon dots for multiphoton bioimaging. *J Am Chem Soc*. 2007;129:11318-11319.
8. Zhu S, Meng Q, Wang L, et al. Highly photoluminescent carbon dots for multicolor patterning, sensors, and bioimaging. *Angew Chem Int Ed*. 2013;52:3953-3957.
9. Liu S, Zhao N, Cheng Z, Liu H. Amino-functionalized green fluorescent carbon dots as surface energy transfer biosensors for hyaluronidase. *Nanoscale*. 2015;7:6836-6842.
10. Xiong C, Liang W, Wang H, et al. In situ electro-polymerization of nitrogen doped carbon dots and their application in an electrochemiluminescence biosensor for the detection of intracellular lead ions. *Chem Commun*. 2016;52:5589-5592.
11. Cui X, Zhu L, Wu J, et al. A fluorescent biosensor based on carbon dots-labeled oligodeoxyribonucleotide and graphene oxide for mercury(II) detection. *Biosens Bioelectron*. 2015;63:506-512.
12. Wang Q, Huang X, Long Y, et al. Hollow luminescent carbon dots for drug delivery. *Carbon*. 2013;59:192-199.
13. Feng T, Ai X, An G, Yang P, Zhao Y. Correction to charge-convertible carbon dots for imaging-guided drug delivery with enhanced in vivo cancer therapeutic efficiency. *ACS Nano*. 2016;10:5587.
14. Zeng Q, Shao D, He X, et al. Carbon dots as a trackable drug delivery carrier for localized cancer therapy in vivo. *J Mater Chem B*. 2016;4:5119-5126.
15. Peng Z, Miyanji EH, Zhou Y, et al. Carbon dots: promising biomaterials for bone-specific imaging and drug delivery. *Nanoscale*. 2017;9:17533-17543.
16. Zhou B, Guo Z, Lin Z, Zhang L, Jiang BP, Shen XC. Recent insights into near-infrared light-responsive carbon dots for bioimaging and cancer phototherapy. *Inorg Chem Front*. 2019;6:1116-1128.
17. Jiang B-P, Zhou B, Lin Z, Liang H, Shen X-C. Recent advances in carbon nanomaterials for cancer phototherapy. *Chem Eur J*. 2019;25:3993-4004.
18. Zhang M, Wang W, Zhou N, et al. Near-infrared light triggered photo-therapy, in combination with chemotherapy using magnetofluorescent carbon quantum dots for effective cancer treating. *Carbon*. 2017;118:752-764.
19. Meng X, Chang Q, Xue C, Yang J, Hu S. Full-colour carbon dots: from energy-efficient synthesis to concentration-dependent photoluminescence properties. *Chem Commun*. 2017;53:3074-3077.
20. Wei J-S, Song T-B, Zhang P, Niu XQ, Chen XB, Xiong HM. A new generation of energy storage electrode materials constructed from carbon dots. *Mater Chem Front*. 2020;4:729-749.
21. Narayanan R, Deepa M, Srivastava AK. Förster resonance energy transfer and carbon dots enhance light harvesting in a solid-state quantum dot solar cell. *J Mater Chem A*. 2013;1:3907-3918.
22. Choi H, Ko S-J, Choi Y, et al. Versatile surface plasmon resonance of carbon-dot-supported silver nanoparticles in polymer optoelectronic devices. *Nat Photonics*. 2013;7:732-738.
23. Wang Y, Liu X, Han X, et al. Unique hole-accepting carbon-dots promoting selective carbon dioxide reduction nearly 100% to methanol by pure water. *Nat Commun*. 2020;11:2531.
24. Yuan F, Wang Y-K, Sharma G, et al. Bright high-colour-purity deep-blue carbon dot light-emitting diodes via efficient edge amination. *Nat Photonics*. 2020;14:171-176.
25. Hu C, Li M, Qiu J, Sun Y-P. Design and fabrication of carbon dots for energy conversion and storage. *Chem Soc Rev*. 2019;48:2315-2337.

26. Feng T, Tao S, Yue D, Zeng Q, Chen W, Yang B. Recent advances in energy conversion applications of carbon dots: from optoelectronic devices to electrocatalysis. *Small*. 2020; 16:2001295.
27. Dhenadhayalan N, Lin K-C, Saleh TA. Recent advances in functionalized carbon dots toward the design of efficient materials for sensing and catalysis applications. *Small*. 2020; 16:1905767.
28. Fernando KAS, Sahu S, Liu Y, et al. Carbon quantum dots and applications in photocatalytic energy conversion. *ACS Appl Mater Interfaces*. 2015;7:8363-8376.
29. Cao L, Shiral Fernando KA, Liang W, et al. Carbon dots for energy conversion applications. *J Appl Phys*. 2019;125:220903.
30. De B, Karak N. A green and facile approach for the synthesis of water soluble fluorescent carbon dots from banana juice. *RSC Adv*. 2013;3:8286-8290.
31. Molaei MJ. Carbon quantum dots and their biomedical and therapeutic applications: a review. *RSC Adv*. 2019;9: 6460-6481.
32. Wang R, Lu K-Q, Tang Z-R, Xu Y-J. Recent progress in carbon quantum dots: synthesis, properties and applications in photocatalysis. *J Mater Chem A*. 2017;5:3717-3734.
33. Zhang M, Bai L, Shang W, et al. Facile synthesis of water-soluble, highly fluorescent graphene quantum dots as a robust biological label for stem cells. *J Mater Chem*. 2012;22: 7461-7467.
34. Sk MA, Ananthanarayanan A, Huang L, Lim KH, Chen P. Revealing the tunable photoluminescence properties of graphene quantum dots. *J Mater Chem C*. 2014;2:6954-6960.
35. Gao N, Huang L, Li T, et al. Application of carbon dots in dye-sensitized solar cells: a review. *J Appl Polym Sci*. 2020; 137:48443.
36. Sharma K, Sharma V, Sharma SS. Dye-sensitized solar cells: fundamentals and current status. *Nanoscale Res Lett*. 2018;13: 381.
37. Martindale BCM, Hutton GAM, Caputo CA, et al. Enhancing light absorption and charge transfer efficiency in carbon dots through graphitization and core nitrogen doping. *Angew Chem Int Ed*. 2017;56:6459-6463.
38. Tetsuka H, Nagoya A, Fukusumi T, Matsui T. Molecularly designed, nitrogen-functionalized graphene quantum dots for optoelectronic devices. *Adv Mater*. 2016;28:4632-4638.
39. Yang G, Wu C, Luo X, et al. Exploring the emissive states of heteroatom-doped graphene quantum dots. *J Phys Chem C*. 2018;122:6483-6492.
40. Shen J, Zhu Y, Yang X, Zong J, Zhang J, Li C. One-pot hydrothermal synthesis of graphene quantum dots surface-passivated by polyethylene glycol and their photoelectric conversion under near-infrared light. *New J Chem*. 2012;36: 97-101.
41. Resch-Genger U, Grabolle M, Cavaliere-Jaricot S, Nitschke R, Nann T. Quantum dots versus organic dyes as fluorescent labels. *Nat Methods*. 2008;5:763-775.
42. Tan M, Zhang L, Tang R, et al. Enhanced photoluminescence and characterization of multicolor carbon dots using plant soot as a carbon source. *Talanta*. 2013;115:950-956.
43. Liu Y, Zhou L, Li Y, Deng R, Zhang H. Highly fluorescent nitrogen-doped carbon dots with excellent thermal and photo stability applied as invisible ink for loading important information and anti-counterfeiting. *Nanoscale*. 2017;9:491-496.
44. Li H, He X, Kang Z, et al. Water-soluble fluorescent carbon quantum dots and photocatalyst design. *Angew Chem Int Ed*. 2010;49:4430-4434.
45. Park Y, Yoo J, Lim B, Kwon W, Rhee SW. Improving the functionality of carbon nanodots: doping and surface functionalization. *J Mater Chem A*. 2016;4:11582-11603.
46. Cayuela A, Soriano ML, Carrillo-Carrión C, Valcárcel M. Semiconductor and carbon-based fluorescent nanodots: the need for consistency. *Chem Comm*. 2016;52:1311-1326.
47. Yuan F, Yuan T, Sui L, et al. Engineering triangular carbon quantum dots with unprecedented narrow bandwidth emission for multicolored LEDs. *Nat Commun*. 2018;9:2249.
48. Ding Y, Zhang F, Xu J, et al. Synthesis of short-chain passivated carbon quantum dots as the light emitting layer towards electroluminescence. *RSC Adv*. 2017;7:28754-28762.
49. Tetsuka H, Asahi R, Nagoya A, et al. Optically tunable amino-functionalized graphene quantum dots. *Adv Mater*. 2012;24:5333-5338.
50. Mehta A, D P, Thakur A, Basu S. Enhanced photocatalytic water splitting by gold carbon dot core shell nanocatalyst under visible/sunlight. *New J Chem*. 2017;41:4573-4581.
51. Li H, Liu R, Kong W, et al. Carbon quantum dots with photogenerated proton property as efficient visible light controlled acid catalyst. *Nanoscale*. 2014;6:867-873.
52. Vijila C, Singh SP, Williams E, et al. Relation between charge carrier mobility and lifetime in organic photovoltaics. *J Appl Phys*. 2013;114:184503.
53. Singh R, Pal B. Study of excited charge carrier's lifetime for the observed photoluminescence and photocatalytic activity of CdS nanostructures of different shapes. *J Mol Catal A: Chem*. 2013;371:77-85.
54. Zhang L, Zhou M, Zhang Z, et al. Ultra-long photoluminescence lifetime in an inorganic halide perovskite thin film. *J Mater Chem A*. 2019;7:22229-22234.
55. Chen T, Chen W-L, Foley BJ, et al. Origin of long lifetime of band-edge charge carriers in organic–inorganic lead iodide perovskites. *Proc Natl Acad Sci U S A*. 2017;114: 7519-7524.
56. Anfimov IM, Kobeleva SP, Pylnev AV, Schemerov IV, Egorov DS, Yurchuk SY. On the problem of determining the bulk lifetime by photoconductivity decay on the unpassivated samples of monocrystalline silicon. *Russ Microelectron*. 2017; 46:585-590.
57. Bscheid C, Engst CR, Eisele I, Kutter C. Minority carrier lifetime measurements for contactless oxidation process characterization and furnace profiling. *Materials*. 2019;12:190.
58. Kiermasch D, Rieder P, Tvingstedt K, Baumann A, Dyakonov V. Improved charge carrier lifetime in planar perovskite solar cells by bromine doping. *Sci Rep*. 2016;6:39333.
59. Varma RS, Thorat N, Fernandes R, Kothari DC, Patel N, Miotello A. Dependence of photocatalysis on charge carrier separation in Ag-doped and decorated TiO_2 nanocomposites. *Catal Sci Technol*. 2016;6:8428-8440.
60. Zhang P, Wang T, Chang X, Gong J. Effective charge carrier utilization in photocatalytic conversions. *Acc Chem Res*. 2016; 49:911-921.

61. Khan R, Ali-Löytty H, Saari J, et al. Optimization of photogenerated charge carrier lifetimes in ALD grown TiO_2 for photonic applications. *Nanomaterials*. 2020;10:1567.
62. Bhattacharyya S, Ehrat F, Urban P, et al. Effect of nitrogen atom positioning on the trade-off between emissive and photocatalytic properties of carbon dots. *Nat Commun*. 2017;8:1401.
63. Kong W, Zhang X, Liu S, et al. N doped carbon dot modified WO_3 nanoflakes for efficient photoelectrochemical water oxidation. *Adv Mater Interfaces*. 2019;6:1801653.
64. Tsai K-A, Hsieh P-Y, Lai T-H, et al. Nitrogen-doped graphene quantum dots for remarkable solar hydrogen production. *ACS Appl Energy Mater*. 2020;3:5322-5332.
65. Luo H, Dimitrov S, Daboczi M, et al. Nitrogen-doped carbon dots/TiO_2 nanoparticle composites for photoelectrochemical water oxidation. *ACS Appl Nano Mater*. 2020;3:3371-3381.
66. Hu S, Chang Q, Lin K, Yang J. Tailoring surface charge distribution of carbon dots through heteroatoms for enhanced visible-light photocatalytic activity. *Carbon*. 2016;105:484-489.
67. Xu H, Yan L, Yu Y, Xu Y. Facile synthesis of carbon-supported silver nanoparticles for optical limiting. *Appl Surf Sci*. 2018;457:655-661.
68. Scharl T, Cadranel A, Haines P, et al. Fine-tuning the assemblies of carbon nanodots and porphyrins. *Chem Commun*. 2018;54:11642-11644.
69. Wang Z, Long P, Feng Y, Qin C, Feng W. Surface passivation of carbon dots with ethylene glycol and their high-sensitivity to Fe^{3+}. *RSC Adv*. 2017;7:2810-2816.
70. Arcudi F, Strauss V, Đorđević L, Cadranel A, Guldi DM, Prato M. Porphyrin antennas on carbon nanodots: excited state energy and electron transduction. *Angew Chem Int Ed*. 2017;56:12097-12101.
71. Wu W, Zhan L, Fan W, et al. Cu–N dopants boost electron transfer and photooxidation reactions of carbon dots. *Angew Chem Int Ed*. 2015;54:6540-6544.
72. Choi Y, Ryu GH, Min SH, et al. Interface-controlled synthesis of heterodimeric silver–carbon nanoparticles derived from polysaccharides. *ACS Nano*. 2014;8:11377-11385.
73. Kainth S, Maity B, Basu S. Label-free detection of creatinine using nitrogen-passivated fluorescent carbon dots. *RSC Adv*. 2020;10:36253-36264.
74. Ferrer-Ruiz A, Scharl T, Haines P, et al. Exploring tetrathiafulvalene–carbon nanodot conjugates in charge transfer reactions. *Angew Chem Int Ed*. 2018;57:1001-1005.
75. Lan M, Di Y, Zhu X, et al. A carbon dot-based fluorescence turn-on sensor for hydrogen peroxide with a photo-induced electron transfer mechanism. *Chem Commun*. 2015;51:15574-15577.
76. Briscoe J, Marinovic A, Sevilla M, Dunn S, Titirici M. Biomass-derived carbon quantum dot sensitizers for solid-state nanostructured solar cells. *Angew Chem Int Ed*. 2015;54:4463-4468.
77. Gao P, Ding K, Wang Y, et al. Crystalline Si/graphene quantum dots heterojunction solar cells. *J Phys Chem C*. 2014;118:5164-5171.
78. Hui W, Yang Y, Xu Q, et al. Red-carbon-quantum-dot-doped SnO_2 composite with enhanced electron mobility for efficient and stable perovskite solar cells. *Adv Mater*. 2020;32:1906374.
79. Zhou Y, Yang S, Yin X, et al. Enhancing electron transport via graphene quantum dot/SnO_2 composites for efficient and durable flexible perovskite photovoltaics. *J Mater Chem A*. 2019;7:1878-1888.
80. Xie J, Huang K, Yu X, et al. Enhanced electronic properties of SnO_2 via electron transfer from graphene quantum dots for efficient perovskite solar cells. *ACS Nano*. 2017;11:9176-9182.
81. Li H, Shi W, Huang W, et al. Carbon quantum dots/TiO_x electron transport layer boosts efficiency of planar heterojunction perovskite solar cells to 19%. *Nano Lett*. 2017;17:2328-2335.
82. Zhang X, Liu C, Li Z, et al. An easily prepared carbon quantum dots and employment for inverted organic photovoltaic devices. *Chem Eng J*. 2017;315:621-629.
83. Zhang X, Li Z, Zhang Z, et al. Efficiency improvement of organic solar cells via introducing combined anode buffer layer to facilitate hole extraction. *J Phys Chem C*. 2016;120:13954-13962.
84. Moon BJ, Lee KS, Shim J, et al. Enhanced photovoltaic performance of inverted polymer solar cells utilizing versatile chemically functionalized ZnO@graphene quantum dot monolayer. *Nano Energy*. 2016;20:221-232.
85. Lin X, Yang Y, Nian L, et al. Interfacial modification layers based on carbon dots for efficient inverted polymer solar cells exceeding 10% power conversion efficiency. *Nano Energy*. 2016;26:216-223.
86. Park S, Lee H, Park SW, et al. Improved exciton dissociation efficiency by a carbon-quantum-dot doped workfunction modifying layer in polymer solar cells. *Curr Appl Phys*. 2021;21:140-146.
87. Kim JK, Park MJ, Kim SJ, et al. Balancing light absorptivity and carrier conductivity of graphene quantum dots for high-efficiency bulk heterojunction solar cells. *ACS Nano*. 2013;7:7207-7212.
88. Kim JK, Kim SJ, Park MJ, et al. Surface-engineered graphene quantum dots incorporated into polymer layers for high performance organic photovoltaics. *Sci Rep*. 2015;5:14276.
89. Benetti D, Jokar E, Yu C-H, et al. Hole-extraction and photostability enhancement in highly efficient inverted perovskite solar cells through carbon dot-based hybrid material. *Nano Energy*. 2019;62:781-790.
90. Yeh T-F, Teng C-Y, Chen S-J, Teng H. Nitrogen-doped graphene oxide quantum dots as photocatalysts for overall water-splitting under visible light illumination. *Adv Mater*. 2014;26:3297-3303.
91. Choi Y, Jeon D, Choi Y, Ryu J, Kim B-S. Self-assembled supramolecular hybrid of carbon nanodots and polyoxometalates for visible-light-driven water oxidation. *ACS Appl Mater Interfaces*. 2018;10:13434-13441.
92. Achilleos DS, Yang W, Kasap H, et al. Solar reforming of biomass with homogeneous carbon dots. *Angew Chem Int Ed*. 2020;59:18184-18188.
93. Martindale BCM, Joliat E, Bachmann C, Alberto R, Reisner E. Clean donor oxidation enhances the H_2 evolution activity of a carbon quantum dot–molecular catalyst photosystem. *Angew Chem Int Ed*. 2016;55:9402-9406.
94. Mas N, Hueso JL, Martinez G, et al. Laser-driven direct synthesis of carbon nanodots and application as sensitizers for visible-light photocatalysis. *Carbon*. 2020;156:453-462.

95. Wu J, Ma S, Sun J, et al. A metal-free electrocatalyst for carbon dioxide reduction to multi-carbon hydrocarbons and oxygenates. *Nat Commun*. 2016;7:13869.
96. Van Tam T, Kang SG, Babu KF, Oh ES, Lee SG, Choi WM. Synthesis of B-doped graphene quantum dots as a metal-free electrocatalyst for the oxygen reduction reaction. *J Mater Chem A*. 2017;5:10537-10543.
97. Rosso C, Filippini G, Prato M. Use of Nitrogen-doped carbon nanodots for the photocatalytic fluoroalkylation of organic compounds. *Chem Eur J*. 2019;25:16032-16036.
98. Li W, Liu Y, Wu M, et al. Carbon-quantum-dots-loaded ruthenium nanoparticles as an efficient electrocatalyst for hydrogen production in alkaline media. *Adv Mater*. 2018;30:1800676.
99. Zou J-P, Wang L-C, Luo J, et al. Synthesis and efficient visible light photocatalytic H_2 evolution of a metal-free g-C_3N_4/graphene quantum dots hybrid photocatalyst. *Appl Catal B*. 2016;193:103-109.
100. Shao L, Yu Z, Li X, Li X, Zeng H, Feng X. Carbon nanodots anchored onto the metal-organic framework NH_2-MIL-88B (Fe) as a novel visible light-driven photocatalyst: photocatalytic performance and mechanism investigation. *Appl Surf Sci*. 2020;505:144616.
101. Wu W, Zhang Q, Wang R, et al. Synergies between unsaturated Zn/Cu doping sites in carbon dots provide new pathways for photocatalytic oxidation. *ACS Catal*. 2018;8:747-753.
102. Guo S, Zhao S, Wu X, et al. A Co_3O_4-CDots-C_3N_4 three component electrocatalyst design concept for efficient and tunable CO_2 reduction to syngas. *Nat Commun*. 2017;8:1828.
103. Ye K-H, Wang Z, Gu J, et al. Carbon quantum dots as a visible light sensitizer to significantly increase the solar water splitting performance of bismuth vanadate photoanodes. *Energy Environ Sci*. 2017;10:772-779.
104. Pan D, Xi C, Li Z, et al. Electrophoretic fabrication of highly robust, efficient, and benign heterojunction photoelectrocatalysts based on graphene-quantum-dot sensitized TiO_2 nanotube arrays. *J Mater Chem A*. 2013;1:3551-3555.
105. Shi W, Zhang X, Brillet J, et al. Significant enhancement of the photoelectrochemical activity of WO_3 nanoflakes by carbon quantum dots decoration. *Carbon*. 2016;105:387-393.
106. Wang F, Chen D, Hu Z, Qin L, Sun X, Huang Y. In situ decoration of CuSCN nanorod arrays with carbon quantum dots for highly efficient photoelectrochemical performance. *Carbon*. 2017;125:344-351.
107. Chen D, Dai S, Su X, et al. N-doped nanodots/np^+-Si photocathodes for efficient photoelectrochemical hydrogen generation. *Chem Commun*. 2015;51:15340-15343.
108. Li M, Zhao R, Su Y, Yang Z, Zhang Y. Carbon quantum dots decorated Cu_2S nanowire arrays for enhanced photoelectrochemical performance. *Nanoscale*. 2016;8:8559-8567.
109. Zhang Z, Lin S, Li X, Li H, Cui W. Metal free and efficient photoelectrocatalytic removal of organic contaminants over g-C_3N_4 nanosheet films decorated with carbon quantum dots. *RSC Adv*. 2017;7:56335-56343.
110. Zhang P, Wang T, Chang X, Zhang L, Gong J. Synergistic cocatalytic effect of carbon nanodots and Co_3O_4 nanoclusters for the photoelectrochemical water oxidation on hematite. *Angew Chem Int Ed*. 2016;55:5851-5855.
111. Liu X, Dai L. Carbon-based metal-free catalysts. *Nat Rev Mater*. 2016;1:16064.
112. Han M, Zhu S, Lu S, et al. Recent progress on the photocatalysis of carbon dots: classification, mechanism and applications. *Nano Today*. 2018;19:201-218.

AUTHOR BIOGRAPHIES

Namhee Kim is currently an MS/PhD student in Prof. Byeong-Su Kim's group in the Department of Chemistry at Yonsei University. She received her BS degree from the Department of Chemistry at Chungnam National University, Republic of Korea, in 2020. Her research interests include nanomaterials and polymers for energy conversion.

Jiyoung Lee is currently a PhD student in Prof. Byeong-Su Kim's group in the Department of Chemistry at Yonsei University. She received her BS and MS degrees from the Department of Chemistry at Soongsil University, Republic of Korea, in 2018 and 2020 under the supervision of Prof. Ik-Soo Shin. Her research interests include nanomaterials and polymers for energy conversion.

Minsu Gu is an assistant professor in the Department of Chemical Engineering at Dong-A University, Republic of Korea. He received his BS degree from the School of Nano-Bioscience and Chemical Engineering at the Ulsan National Institute of Science and Technology (UNIST), Republic of Korea, in 2013, and his PhD degree from the Department of Energy Engineering at UNIST in 2018 under the supervision of Prof. Byeong-Su Kim. He was a postdoctoral researcher in Dr. Allen J. Bard's group in the Department of Chemistry at the University of Texas at Austin. His research interests include the electrochemistry of functional nanomaterials and polymers for energy conversion and storage applications.

Byeong-Su Kim is a professor in the Department of Chemistry at Yonsei University, Republic of Korea. He received his BS and MS degrees in Chemistry at Seoul National University and his PhD degree in Chemistry at the University of Minnesota, Twin Cities, in 2007. After his postdoctoral research at MIT, he

started his independent career at UNIST in 2009 and recently moved to Yonsei University in 2018. His group investigated a broad range of topics in macromolecular chemistry for the study of novel polymer and hybrid nanomaterials, including the molecular design and synthesis of self-assembled polymers and carbon-based nanostructures.

How to cite this article: Kim N, Lee J, Gu M, Kim B-S. Modulating charge carriers in carbon dots toward efficient solar-to-energy conversion. *Carbon Energy*. 2021;1-25.
https://doi.org/10.1002/cey2.115